Geochemistry 80 (2020) 125612

Contents lists available at ScienceDirect

Geochemistry

journal homepage: www.elsevier.com/locate/chemer

Rare earth element (REE) enrichment of the late Ediacaran Kalyus Beds (East European Platform) through diagenetic uptake

Ion Francovschi[a], Eugen Grădinaru[a,*], Relu-Dumitru Roban[a,*], Mihai N. Ducea[a,b], Valerian Ciobotaru[c], Leonid Shumlyanskyy[d,e]

[a] University of Bucharest, Faculty of Geology and Geophysics, Bucharest, Romania
[b] Department of Geosciences, University of Arizona, Tucson, AZ, USA
[c] Institute of Geology and Seismology, Chişinău, Republic of Moldova
[d] M.P. Semenenko Institute of Geochemistry, Mineralogy and Ore Formation, Kyiv, Ukraine
[e] School of Earth and Planetary Sciences, Curtin University, Perth, Australia

ARTICLE INFO

Handling Editor: Carita Augustsson

Keywords:
Geochemistry
Ce anomaly
Y/Ho
Diagenesis
Republic of Moldova

ABSTRACT

The Kalyus Beds of the late Ediacaran Nagoryany Formation occurring in the northeastern part of the Republic of Moldova are dominated by black argillites with phosphorites and calcareous concretions. Four lithological groups were examined with respect to their rare earth element (REE), major and trace element geochemistry: phosphorites, enriched argillites, pure argillites and carbonates. Phosphorites and enriched argillites exhibit a pronounced middle-REE bulge suggesting a strong diagenetic uptake of REEs. Y/Ho ratios are mostly < 35, values that are consistent with derivation of > 90% of REEs from lithogenous sources. Pure argillites show a flat REE distribution similar to that of average upper continental crust (UCC), indicating that REEs are likely related to detrital siliciclastics derived from felsic to mafic source rocks of the adjacent regions of Baltica, which was isolated within paleo-oceans during the late Ediacaran. Carbonates show a light-REE depleted pattern with relatively high Y/Ho ratios (up to 53) that suggests the preservation of a predominantly hydrogenous (seawater-derived) REE signal. Ce/Ce* ratios of ~0.80–1.02 reflect suboxic to anoxic seawater conditions. This is a locally and temporally constrained anoxic event, since widespread oxic conditions were specific for the continental margins of Baltica. The phosphorites and enriched argillites groups of the Kalyus Beds show high middle-REE enrichment comparable to those of other known world phosphorite deposits. Their total REE contents are high (793–1735 ppm) and are of potential economic interest. These results provide insights for expanding global REE exploration targets and may have implications for a better understanding of the depositional environments during the late Ediacaran.

1. Introduction

Interpretation of depositional environments of ancient sediments and, in particular, their paleo-redox conditions is a fundamental task in basin analysis. A variety of approaches is used to define depositional conditions, one of them being geochemical investigations. Rare earth elements (REEs) are routinely used in assessing variations in paleo-seawater chemistry and/or terrigenous sediment fluxes. Among the parameters preserving a seawater signature, the Ce (cerium) anomaly can provide information about redox conditions of the depositional environment (Elderfield, 1988; German and Elderfield, 1990; Zhao et al., 2013) while the Eu (europium) anomaly can indicate the origin of REE input (Condie, 2001; Kidder et al., 2003; Zhou et al., 2005). REEs are of crucial importance for technology industries with increasing demand for REEs driven by innovations in the emerging technologies sector, in particular – green energy, permanent magnets and electronic industries (Humphries, 2010; Goonan, 2011; Christmann, 2014). Therefore, a detailed understanding of the processes of accumulation of REEs is valuable to exploration and extraction.

Numerous REE studies have identified several general types of REE patterns (e.g. McArthur and Walsh, 1984; Kidder and Eddy-Dillek, 1994; Felitsyn and Morad, 2002; Abedini et al., 2011; Abedini and Calagari, 2015; Chen et al., 2015). Relative to the average of the upper continental crust (UCC), characteristic REE distribution patterns are: (1) a 'flat distribution' signifying predominantly terrigenous siliciclastic influence, (2) a 'middle-REE bulge' probably due to post-depositional

* Corresponding authors at: University of Bucharest, Faculty of Geology and Geophysics, RO-010041, Bucharest, Romania.
E-mail addresses: eugen.gradinaru@g.unibuc.ro (E. Grădinaru), reludumitru.roban@g.unibuc.ro (R.-D. Roban).

https://doi.org/10.1016/j.chemer.2020.125612
Received 5 October 2019; Received in revised form 17 February 2020; Accepted 19 February 2020

modification of primary patterns by diagenetic processes and (3) a 'heavy-REE enrichment' indicative of seawater (hydrogenous) influence (Haley et al., 2004; Kim et al., 2012). All patterns used in this paper are normalized to the REE composition of average upper continental crust of Taylor and McLennan (1985), which is most commonly used in the literature, even though slightly different, newer estimates of UCC (e.g. Rudnick and Gao, 2003) exist in the literature.

We determined the concentrations of REEs, major and trace elements of various lithologies of the late Ediacaran Kalyus Beds in the Naslavcea section of northern Moldova with two aims: (1) to determine the provenance of REEs in this section, and (2) to understand the factors which led to middle-REE enrichment. The Naslavcea section is well suited for a detailed study of this topic because it contains several different lithological types, thus allowing assessment of lithologic influences on REE contents. The results of this study have implications for Ediacaran paleomarine conditions and diagenetic processes but also for evaluation of REE provenance in phosphorites.

2. Geological background

2.1. Stratigraphic framework and dating of the Kalyus Beds

The study section is located in the southwestern part of the East European Platform, within the Republic of Moldova (Fig. 1). The Dniester River region, which extends both in Ukraine and the Republic of Moldova, comprises one of the most important Ediacaran macrofossil-bearing successions in the world, harbouring accessible and well-preserved outcrops containing abundant multicellular fossils (e.g. Zaika-Novatsky and Palij, 1974; Palij, 1976; Palij et al., 1979; Velikanov et al., 1983; Gnilovskaya et al., 1988; Fedonkin et al., 2007). The lithostratigraphy of the Ediacaran deposits in the Dniester River region includes sedimentary units established in Ukraine (Velikanov, 1979; Velikanov et al., 1983). The lithostratigraphy of the Ediacaran deposits in the Republic of Moldova, which is mainly based on data obtained from boreholes, includes a few additional units (Bukatchuk, 1973; Bukatchuk et al., 1988; Francovschi et al., 2017).

Our study is focused on the late Ediacaran Kalyus Beds, a member of the Nagoryany Formation, exposed in an abandoned quarry located in the vicinity of Naslavcea village, Ocnița county (48°29″ N, 27°34″ E). The Kalyus Beds comprise a monotonous succession of black argillites, having more or less regular layers of phosphorite concretions and calcareous concretions. The thickness of the complete successions of the Kalyus Beds, found only in boreholes, varies between 60–80 m, while the outcrops in the area of the Naslavcea village show erosion-reduced thicknesses of less than 45 m.

In the Dniester River basin, the Kalyus Beds conformably overlie sandstones of the Dzhurzhivka Beds, and are unconformably overlain by sandstones of the Pylypy Beds of the Kanyliv Group (Fig. 2). In the Republic of Moldova, based on data given by Bukatchuk (1973) and Bukatchuk et al. (1988), wells drilled through the Nagoryany

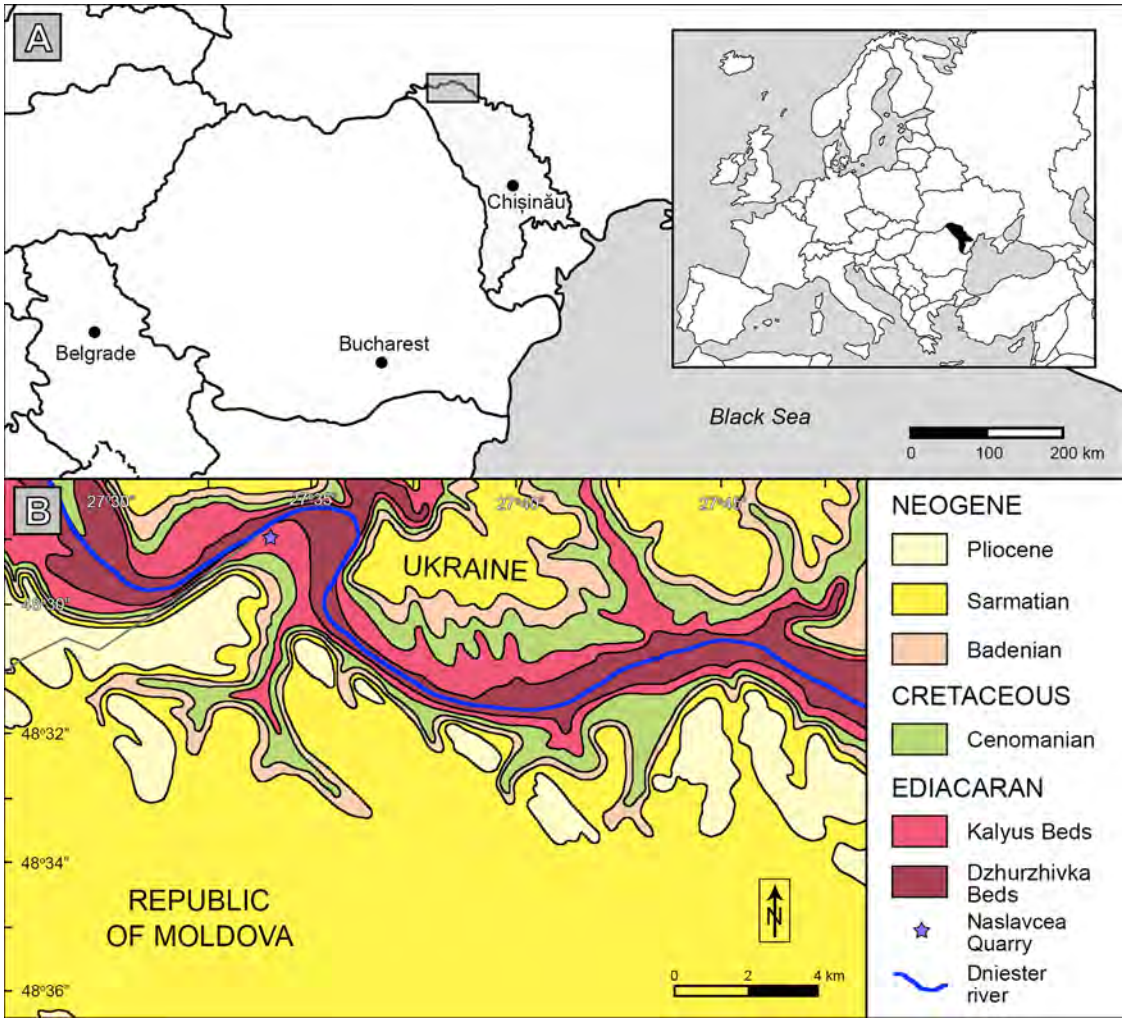

Fig. 1. A. The studied area (inset highlights the Republic of Moldova); B. Geological map of the northeastern part of the Republic of Moldova which includes the location of the Naslavcea Quarry (modified after Bukatchuk et al., 1988).

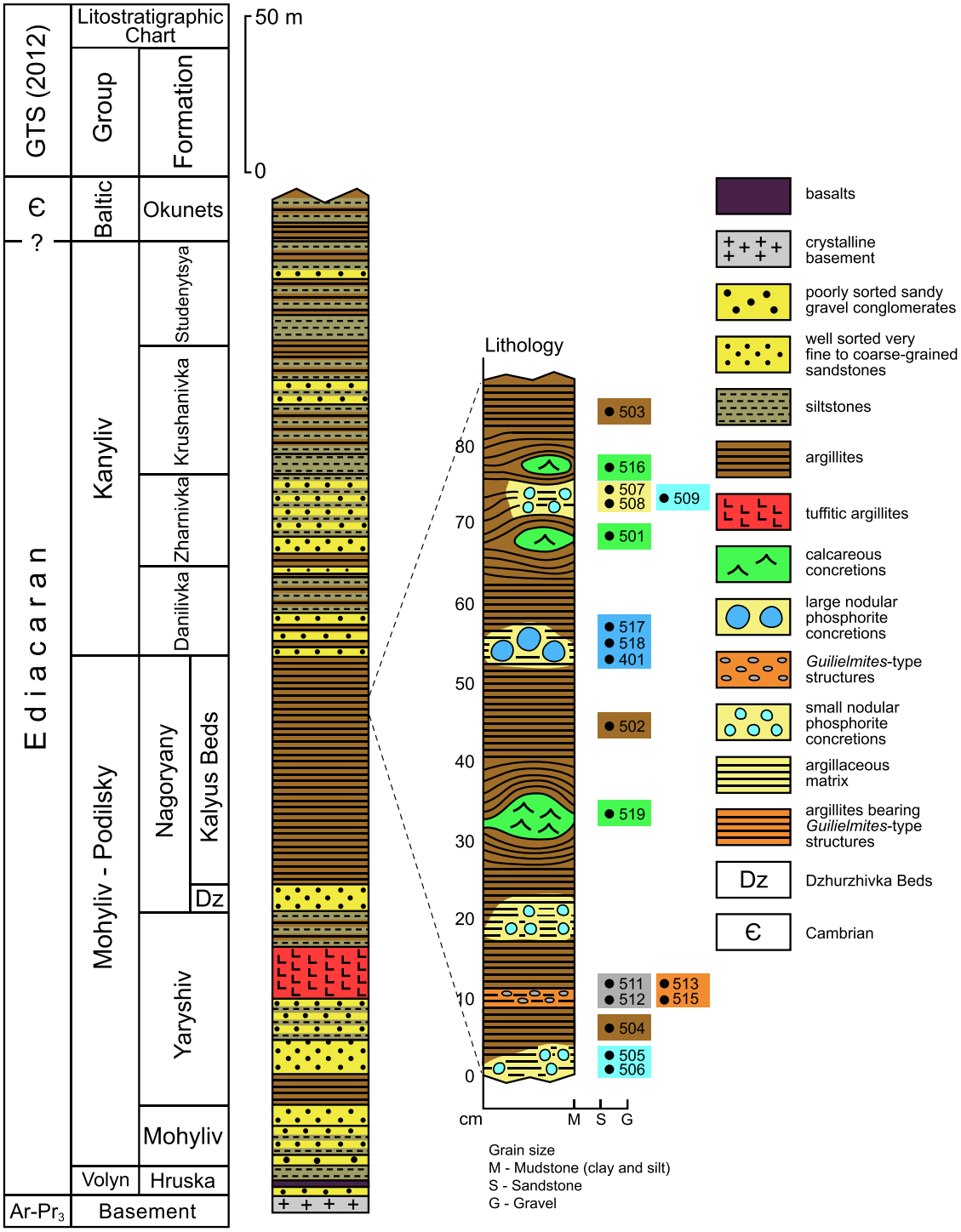

Fig. 2. Lithostratigraphic log of the studied section in the Kalyus Beds in the Naslavcea Quarry, Republic of Moldova. Lithostratigraphic nomenclature after Velikanov (1979).

Formation document a sequence comprising the Dzhurzhivka Beds, Kalyus Beds, with the Sălcuța and Lunguța beds above.

Although the black argillites are the dominant lithological type in the Kalyus Beds, the 88 cm-long studied section in the Naslavcea Quarry (Fig. 2) comprises: (I) black argillites; (II) argillaceous matrices; (III) argillites bearing *Guilielmites*-type structures; (IV) small nodular phosphorite concretions (1–3 cm); (V) large nodular phosphorite concretions (3–15 cm); (VI) *Guilielmites*-type structures, and (VII) calcareous concretions with cone-in-cone structures.

Guilielmites-type structures in the studied section have not been described in the literature. However, some authors have found such structures in boreholes that intercepted the Kalyus Beds, and considered them as *Guilielmites* (Bukatchuk, 1973; Patrulius and Iordan, 1974), a structure of debated origin (e.g. Wood, 1935; Mortelmans, 1957). Interpretation of their corresponding geochemical parameters yields important data on the phosphogenesis processes in the Kalyus Beds. Similar structures have also been found in cores sampled from the Bătrânești borehole (northeastern Romania), 14-Cornești borehole (central Moldova), 1-g Bolotino (northwestern Moldova), suggesting that the conditions controlling the formation of *Guilielmites*-type

structures were regionally extensive. One might consider that these structures could represent precursors of the phosphorite nodular concretions. In the literature, there are no alternative interpretations.

The Kalyus Beds from the Republic of Moldova and Ukraine are dated as late Ediacaran based on fossil content (e.g. Ivantsov et al., 2015; Grazhdankin and Maslov, 2015). The lowermost Mohyliv Formation contains *Dickinsonia* and *Tribrachidium heraldicum* which are diagnostic of late Ediacaran age. At the top of the Ediacaran succession, the Ediacaran – Cambrian boundary is placed between the Studenytsya Formation of the Kanyliv Group and Okunets Formation of the Baltic Group. *Harlaniella podolica* and *Palaeopascichnus delicatus* which are found in the Studenytsya Formation have a relatively short stratigraphic range and both have an upper stratigraphical range close to the Ediacaran – Cambrian boundary. The overlying Okunets Formation has trace fossils typical of the basalmost Cambrian as well as tubular fossils of *Sabellidites cambriensis*, another fossil typical of the basal Cambrian. The Kalyus Beds have a poor fossil record consisting of *Nimbia paula* and vendotaenids. *Nimbia paula* is a morphologically simple form, but not the most typical of late Ediacaran. Vendotaenids are filamentous fossils which are not diagnostic, but consistent with a late Ediacaran age. Recent studies that used precise U-Pb radiometric dating techniques on bentonites (Soldatenko et al., 2019) have shown that the underlying beds of the Yaryshiv and Mohyliv Formations are approximately 555 Ma.

2.2. Paleoenvironmental setting

Gamma Ray log profiles of wells penetrating the Ediacaran Mohyliv-Podilskyi and Kanyliv groups from the southwestern part of the East European Platform (AGMR, 1994), as well as data from several outcrops in the middle course of the Dniester River, highlight several stacked coarsening-upward sequences. The more argillaceous sequences contain diverse assemblages of carbonaceous algae (*Vendotaenia*) and acritarchs (Aseeva, 1976; Gnilovskaya et al., 1988) indicative of an inner to outer shelf, peritidal to intertidal depositional environment. Wave cross-stratification in sandstones interbedded within the Mohyliv-Podilskyi Group, and the lower part of the Kanyliv Group, suggest a shoreface depositional environment. The cyclic, coarsening-upward sequences observed throughout the stratigraphic succession thus reflect repeated advances and retreats of the shoreline in response to the rise and fall of relative sea level. There is little indication of regional tectonic activity during this interval (Bukatchuk et al., 1988), and therefore eustacy is considered to have been the primary factor controlling sea level.

Estimates of water depth during deposition of the Kalyus black argillites have been somewhat inconsistent. Early workers (Văscăuțanu and Savul, 1927; Văscăuțanu, 1931) interpreted the black argillites as shallow lagoonal deposits. Văscăuțanu considered that shallow lagoonal deposits allowed the accumulation of phosphatic material, as well as terrigenous material derived from the land. Consequently, this led to the formation of nodular phosphorite concretions within the argillites. These were later reinterpreted as open-marine environments in the outer shelf zone (Kopeliovich, 1965; Bukatchuk, 1973; Velikanov et al., 1983; Bukatchuk et al., 1988). According to this latter interpretation, the phosphorites-bearing black argillites were deposited beneath the pycnocline, in association with upwelling currents and detrital siliciclastic material derived from the land (Bukatchuk et al., 1988).

3. Methods

3.1. Field and petrographic methods

Based on data concerning the REE and non-REE contents, which will be discussed later, the lithological types can be assigned to four distinct groups: (A) small nodular phosphorite concretions (Figs. 3A, 3B and 4A) and large nodular phosphorite concretions (Fig. 3C) – phosphorites group; (B) argillaceous matrix (Figs. 3B and 4A) and argillites bearing *Guilielmites*-type structures (Figs. 3A and 4B) – enriched argillites group; (C) calcareous concretions with cone-in-cone structures (Figs. 3B and 4A) – carbonates group; (D) argillites (Figs. 3A, 3B and 4A) and *Guilielmites*-type structures (Figs. 3A and 4B) – pure argillites group. In order to obtain reliable results which would help yield a complex view of the geochemical characteristics of the Kalyus Beds, two to three samples were taken from each lithological type. Fresh representative samples (three small nodular phosphorite concretions – samples 505, 506, 509; three large nodular phosphorite concretions – samples 517, 518, 401; two *Guilielmites*-type structures – samples 511, 512; three argillites – samples 502, 503, 504; two argillaceous matrices – samples 507, 508; two argillites bearing *Guilielmites*-type structures – samples 513, 515; and three calcareous concretions – samples 501, 516, 519) were taken at regular intervals and prepared for analyses. Rock samples were crushed to a fine powder using a pulveriser or a mortar and pestle. The powders were used for ICP-MS and XRF analyses.

The petrographic composition was studied by standard optical methods in the Department of Mineralogy, University of Bucharest. Nodular phosphorite concretions, *Guilielmites*-type structures and calcareous concretions samples were selected for the preparation of polished sections (30 μm thickness).

3.2. ICP-MS methods

Rare earth elements (REEs) and other trace elements were measured in solution mode using a Thermo Element X-Series II single collector ICP-MS at the University of Arizona, USA (Rossel et al., 2013). Approximately 5 mg of representative sample were dissolved in about 7 ml of concentrated HF-HNO_3 mixtures, dried down and re-dissolved in a mild 1% nitric acid before being analysed. Several 1–10 ppm internal standards were used for different elements. Columbia River Basalt material standard material was used as an external standard. Analysis routines involved 30 individual measurements. Typical analytical errors are 3–5% of the reported values, whereas the detection limits of the ICP-MS measurements for all measured elements are well below the analysed values, typically in the ppt or sub ppt range; in other words, the detection limits in the ICP-MS are millions to hundreds of million times below the measured values. Several dilution steps were undertaken for some of the samples, given the high concentration of the REEs.

3.3. XRF methods

Major element concentrations were analysed using an Epsilon 1 EDXRF Spectrometer. Approximately 30 mg of sample was carefully crushed to a fine powder and put into capsules before being analysed. Standard reference materials (such as BHVO-2-NP, Apatite-NP, Mica-Mg-NP, RS3-NP, GH-NP) and internal control samples were analysed with each sample batch to monitor analytical accuracy and precision. The mean deviation of the results from the standards was typically better than 5% for most elements and better than 10% for alkaline earth elements.

3.4. SEM-EDS analysis

Scanning electron microscopy and energy dispersive spectroscopy (SEM-EDS) were performed on a representative calcareous concretion sample with the diameter of 5.8 cm, using a scanning electron microscope (Phenom XL), equipped with an energy dispersive X-ray analyzer with a Silicon Drift Detector (SDD). The sample was wrapped in foil so that the surface remained flat during the analysis. The SEM was operated in low-vacuum mode, under a pressure of 60 Pa, with an accelerating voltage of 15 kV. Detailed chemical compositions were obtained from a micro volume via a spot analysis. Multiple spot analyses were taken for each image. This allowed the identification of the main mineral phases present in the sample.

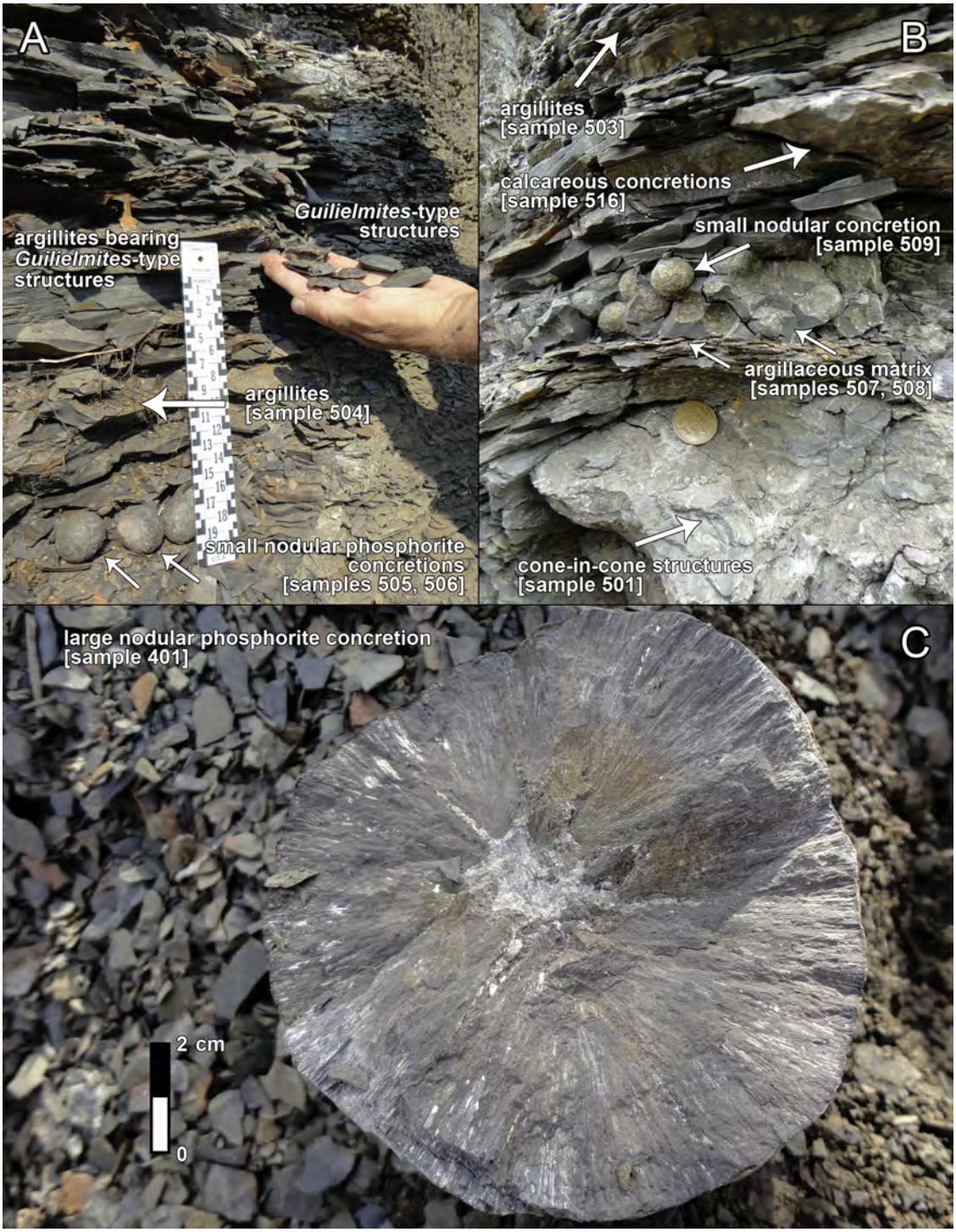

Fig. 3. Representative outcrop photos from the studied section in the Naslavcea Quarry, Republic of Moldova. A – argillites and small nodular phosphorites; B – argillites, calcareous concretions, argillaceous matrix and small nodular phosphorites; C – cracked large nodular phosphorite concretion with a visible radial structure and a rich-$CaCO_3$ core.

3.5. Elemental calculations

The amount of each element in each sample was expressed as an enrichment factor (EF) (Tribovillard et al., 2006):

$$EF_x = (X/Th)_{sample}/(X/Th)_{UCC}$$

where X/Th is Thorium (Th)-normalized concentration of element X, ratio-ed to that of average upper continental crust (UCC) as given in Taylor and McLennan (1985). REE concentrations must be normalized to a detrital element (Th or Al) to correct for variations in detrital concentrations (e.g. Algeo and Maynard, 2004; Tribovillard et al., 2006). Since aluminium (Al) was not analysed in this study, thorium (Th) was used for the normalisation.

The relative enrichments of the light (La, Ce, Pr, Nd), middle (Sm, Eu, Gd, Tb, Dy and Ho) and heavy (Er, Tm, Yb and Lu) REE fractions are reported as ratios: LREE/MREE, LREE/HREE, and MREE/HREE. These ratios were calculated by taking a single element as a proxy for each fraction. The most commonly used proxies for LREE/MREE, LREE/

Fig. 4. Representative outcrop photos from the studied section in the Naslavcea Quarry, Republic of Moldova. A – argillites, calcareous concretions, small nodular phosphorites and argillaceous matrix; B – a concentration of *Guilielmites*-type structures on a bedding surface within argillites.

HREE, and MREE/HREE are La/Sm, La/Yb, and Sm/Yb, respectively (e.g. Bau and Dulski, 1996; Zhang et al., 2016). Another method of evaluating MREE enrichment is the MREE anomaly which is expressed as MREE/MREE* (e.g. Chen et al., 2015):

$$\text{MREE/MREE*} = (2 \times \text{average [MREE]})/(\text{average [LREE]} + \text{average [HREE]}) \quad (1)$$

Ce anomaly (Ce/Ce*) and Eu anomaly (Eu/Eu*) values were quantitatively calculated by using the following equations (Bau and Dulski, 1996), (Taylor and McLennan, 1985):

$$Ce/Ce^* = Ce_N/(0.5La_N + 0.5Nd_N) \quad (2)$$

$$Eu/Eu^* = Eu_N/(0.5Sm_N \times 0.5Gd_N) \quad (3)$$

where N refers to the normalized concentrations to the average upper continental crust (UCC).

4. Results

4.1. Petrographic data

Petrographic examinations of nodular phosphorite concretions show radial growth of brown apatite minerals (Fig. 5D, E, F, G). The nodules incorporated impurities in the form of clay minerals during the process of radial growth (Fig. 5F). Voids that were filled with silica (Fig. 5C, D, F, G, H) or calcite (Fig. 5C, D, E, F, H) indicate that the nodular phosphorite concretions underwent syneresis processes during late diagenesis. In addition, during this phase some apatite crystals were replaced by calcite (Fig. 5D, E) and silica (Fig. 5D) and some calcite crystals were replaced by apatite which exhibits euhedral crystals (Fig. 5C). Pyrite and chalcopyrite are present as anhedral, dispersed and solitary crystals within the matrix (Fig. 5E). Calcareous concretions are characterised by elongated calcite crystals enriched in manganese up to 1 mm in size pressed tightly in between each other and oriented in a

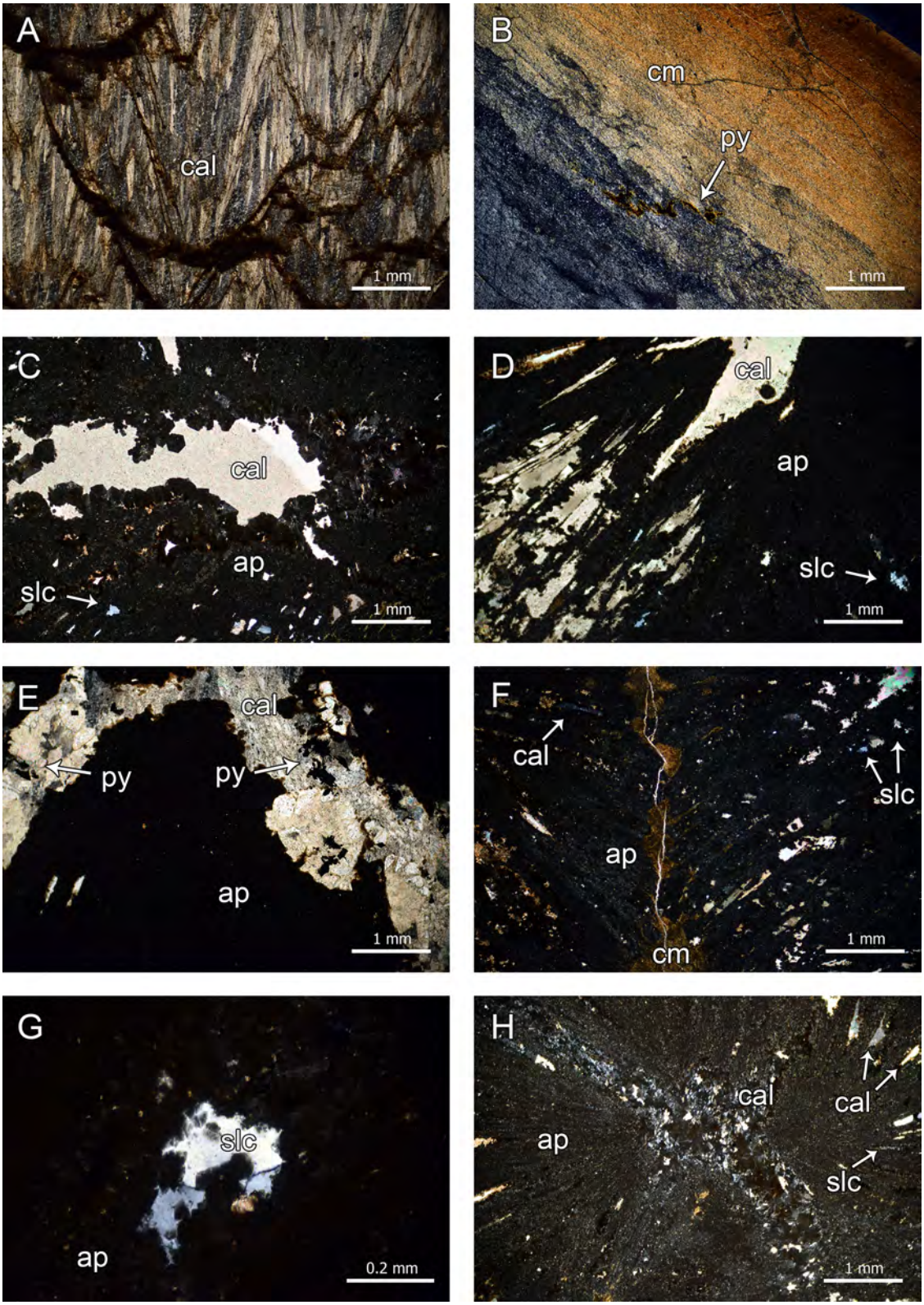

Fig. 5. Microscopic images of polished thin sections of A. calcareous concretions with cone-in-cone structures; B. *Guilielmites*-type structures; C, D, E, G – nodular phosphorite concretions; F – two joined small nodular phosphorite concretions; H – center of a nodular phosphorite concretion; ap – apatite minerals; cal – calcite; slc – silica; py – pyrite; cm – clay minerals. Abbreviations after Whitney and Evans (2010).

single direction (Fig. 5A). These are covered by thin layers of clayey material, in most cases by kaolinite and illite (Fig. 6A, C). The areas with big sized crystals are replaced by smaller crystals at the contact with irregular fractures. The presence of clay minerals as well as organic matter (Fig. 6A) prove that during the growth process in early diagenesis, the calcareous concretions incorporated impurities from the host clays. Sphalerite and pyrite are present as anhedral, dispersed and in most cases solitary crystals, while galena is present as anhedral and

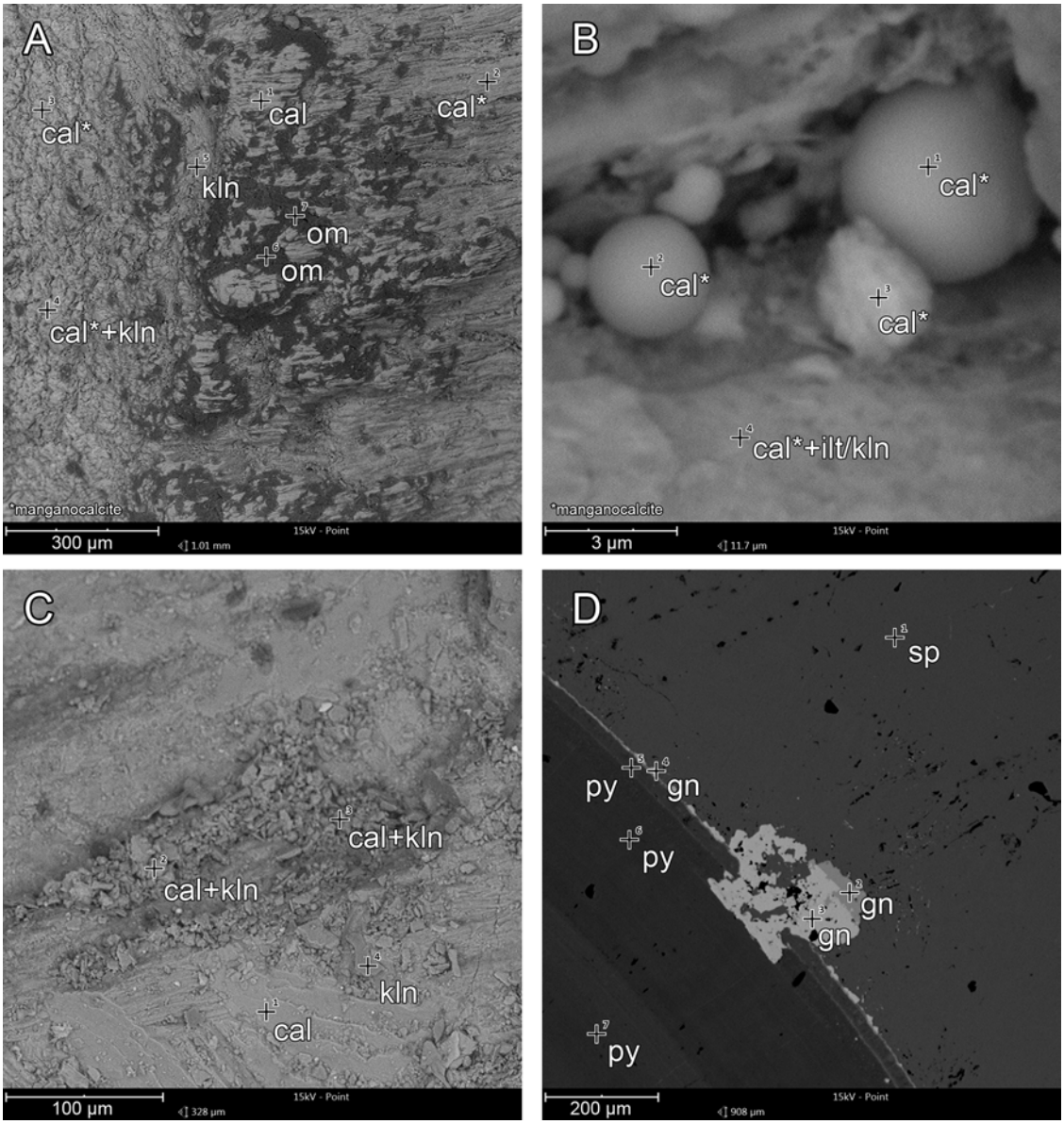

Fig. 6. High resolution SEM images of calcareous concretions. A. manganocalcite mixed with organic matter and, rarely, kaolinite; B. globular manganocalcite with an input of clay minerals (illite/kaolinite); C. aluminosilicates, specifically kaolinite; D. metallic mineralisations such as sphalerite, blenda and pyrite.

veiny crystals within the composition of the matrix (Fig. 6D). These characteristics as well as the irregular form of the calcite granules (Fig. 6A, B, C) suggest that the calcareous concretions formed during diagenesis after the crystallisation of carbonate gels.

Petrographic examinations of argillites (Velikanov et al., 1983; Sokur and Figura, 2009; Sokur, 2010, 2011) point out a dispersed scaly, irregular, parallel or mixed structure. The predominant mineral phases are chlorite-illite-kaolinite. Rarely, authigenic montmorillonite and globular pyrite can be identified. Clastic flakes of biotite as well as fine grains of quartz and zircon are encountered. Recent studies (Sokur, 2010, 2011) have identified carbonates, kaolinite and apatite minerals within the composition of the argillites. The simultaneous presence of clay minerals, carbonates and phosphates underlines the input of allogenic and authigenic material during the sedimentation of the Kalyus Beds. Argillaceous matrices are characterised by the presence of illite, quartz, kaolinite and apatite which are the predominant mineral phases of these lithologies (Sokur, 2010, 2011). These minerals are characterised by finely dispersed material with an insignificant amount of crystalline phases. Macroscopically, the *Guilielmites*-type structures indicate that these are structures similar to nodular phosphorite concretions which failed to incorporate apatite and grow in size. However, petrographic examinations show that clay minerals are the main constituent with rare occurrences of pyrite (Fig. 5B).

Based on microscopic examinations, diagenetic processes influenced the mineralogy and texture of the Kalyus Beds in two separate stages of early and late diagenesis. Presence of voids and incorporation of clay minerals during the growth of the phosphorite concretions and formation of carbonate gels is reckoned to be typical effects of early diagenetic processes. Filling of voids with calcite and silica after dehydration, replacement of apatite by calcite and silica and vice-versa, as well as the formation of cone-in-cone structures in the case of calcareous concretions are interpreted to be the most important effects of the late diagenetic processes in the Kalyus Beds.

4.2. Major elements

Results of the major element analyses obtained in the present study are listed in Table 1. Samples are listed based on the four lithological types.

Table 1
Major element contents in the Ediacaran Kalyus Beds, Naslavcea Quarry, Republic of Moldova (C – calcareous concretions; A – argillites; F – *Guilielmites*-type structures; M – argillaceous matrix; MF – argillites bearing *Guilielmites*-type structures; PS – small nodular phosphorite concretions; PL – large nodular phosphorite concretions).

Sample	501 C	516 C	519 C	502 A	503 A	504 A	511 F	512 F	507 M	508 M	513 MF	515 MF	505 PS	506 PS	509 PS	517 PL	518 PL	401 PL
SiO_2	13.76	12.72	24.12	57.67	56.37	54.19	53.68	57.16	33.56	37.11	42.45	52.52	23.18	14.66	17.72	13.44	8.76	10.95
Al_2O_3	3.88	3.42	7.26	20.43	19.95	20.07	19.40	20.81	10.42	11.68	14.39	18.36	7.00	4.47	7.27	4.69	3.06	5.42
Fe_2O_3	2.39	2.17	3.45	9.70	10.20	10.05	10.49	10.53	6.08	6.63	9.30	10.42	4.97	3.43	5.91	2.58	2.36	2.01
K_2O	0.63	0.59	1.28	3.40	3.70	3.66	3.20	3.55	1.70	1.71	2.26	3.34	1.00	0.61	0.69	0.56	0.34	0.36
CaO	46.06	46.85	37.57	0.41	0.69	0.46	0.33	0.30	20.28	19.54	12.58	2.95	29.99	36.17	31.97	35.06	36.97	36.18
MgO	1.69	1.37	1.38	1.85	1.76	2.02	1.73	2.02	1.63	1.73	1.52	2.45	1.37	0.89	1.23	1.37	0.82	1.51
SO_3	0.19	0.17	0.26	0.29	0.06	0.14	0.06	0.17	0.54	0.59	0.54	0.20	0.77	0.74	0.71	0.33	0.26	0.42
P_2O_5	0.42	0.14	0.27	0.16	0.32	0.16	0.08	0.06	17.33	16.05	9.53	1.74	23.42	26.45	25.02	37.00	39.60	41.66
TiO_2	0.21	0.19	0.42	1.00	0.97	1.00	0.95	0.97	0.50	0.54	0.67	0.93	0.31	0.18	0.19	0.22	0.10	0.11
MnO	1.87	1.90	1.56	0.05	0.05	0.05	0.05	0.05	0.21	0.16	0.06	0.05	0.53	0.77	0.66	0.55	0.73	0.41

Major oxides in the phosphorites group are dominated by CaO, P_2O_5, and SiO_2. The next most abundant elements are Al_2O_3, Fe_2O_3 and MgO. The concentration of all other oxides [TiO_2, K_2O, SO_3 and MnO] is generally low (< 1%). Major element composition reflects the dominance of apatite as the primary mineral in the phosphorites together with subordinate calcite, quartz and clay minerals. P_2O_5 contents vary between 23.42 and 41.66%. The highest P_2O_5 values (up to 41.66%) are recorded in the large nodular phosphorite concretions (Fig. 7A), while the P_2O_5 values in the small nodular phosphorite concretions have values up to 26.5%. MgO contents range from 0.8 to 1.5% compared to a maximum Mg concentration in sedimentary francolite of 0.36% (McArthur, 1985; Jarvis et al., 1994). SiO_2 and Al_2O_3 concentrations show moderate variation (8.76–23.18%, 3.06–8.99% respectively), that reflects the changing properties of quartz (detrital), opal-CT/silica (a product of diagenesis) and mixed clay assemblages in the deposits (Fig. 7A). TiO_2 values vary between 0.10 and 0.31%, and are considered to principally represent clay minerals, as this element shows a positive correlation with Al_2O_3 (r = 0.64). The alkali component K_2O shows minor variability (0.34–0.99%). K_2O content is primarily determined by the type and amount of smectite-illite, glauconite and K-feldspar in the assemblage. Fe_2O_3 contents range from 2.01–5.90%, and show a strong correlation with Al_2O_3 (r = 0.81), indicating an association with terrigenous material. The SO_3 contents range from 0.26 to 0.74% (Fig. 7C). This range of SO_3 contents in the samples is attributable to the presence of sulphides (pyrite, sphalerite), showing a very high correlation with Fe_2O_3 (r = 0.80) and Zn (r = 0.56). MnO contents range from 0.41 to 0.76%.

The pure argillites group is characterised by major oxides which are dominated by SiO_2, Al_2O_3 and Fe_2O_3; K_2O and MgO are the next abundant elements, while the concentrations of all other oxides [TiO_2, CaO, P_2O_5] is lower than 1%. The major element composition reflects the dominance of land-derived terrigenous material, together with subordinate calcite, apatite. SiO_2 and Al_2O_3 concentrations show little variation (53.67–57.67%, 19.39–20.81% respectively), that reflects the unvarying properties of quartz (detrital) and mixed clay assemblages in the deposits (Fig. 7A). SiO_2 shows a high correlation with Al_2O_3 (r = 0.80), meaning silica is associated with detrital clay phases. TiO_2 values vary between 0.95 and 1.00% and show a positive correlation with Al_2O_3 (r = 0.50). These contents are higher than the average value of TiO_2 in the felsic rocks from the Volhyn-Brest continental flood basalt province, but lower than the average value in the mafic rocks from this province (0.74% and 2.29% respectively, Nosova et al., 2008). Fe_2O_3 and K_2O contents range from 9.70 to 10.52% and 3.20–3.70%, respectively (Fig. 7D). MgO contents range from 1.72 to 2.02% compared to a maximum Mg concentration in the average shale of 1.5% (Turekian and Wedepohl, 1961). P_2O_5 contents vary between 0.16 and 0.31%. SO_3 contents are very low and range between 0.06 and 0.29%. MnO contents are negligible and show an average value of 0.05%.

Major oxides in the enriched argillites group are dominated by SiO_2, Al_2O_3 and CaO. The next most abundant elements are P_2O_5, K_2O and MgO. Concentrations of all other oxides [TiO_2, SO_3, MnO] is lower than 1%. The major element composition reflects the combination of land derived detrital clay material and seawater-derived phosphorite-carbonate material. SiO_2 and Al_2O_3 show moderate variation (33.56–52.52%, 10.42–18.36% respectively) that reflects the changing properties of quartz and mixed clay assemblages in the deposits (Fig. 7A). SiO_2 shows a linear correlation with Al_2O_3 (r = 0.99), which points out that virtually all silica is associated with detrital clay phases. P_2O_5 contents vary between 1.74 and 17.32%. The highest P_2O_5 contents (up to 17.3%) are recorded in the argillaceous matrices, while the P_2O_5 contents in the argillites bearing *Guilielmites*-type structures are lower (up to 9.5%). This is expected, since argillaceous matrices encapsulate the P_2O_5-rich phosphorites, while the other lithology encapsulate P_2O_5-poor *Guilielmites*-type structures. This characteristic is also available for the other elements, meaning that allochthonous elements (such as Si, Al, Ti) have higher values in the argillites bearing *Guilielmites*-type structures, while elements from an authigenic source (P, Ca) have higher values in the argillaceous matrices. CaO values vary from 2.95 to 20.28% and show a linear correlation with P_2O_5 (r = 0.99). This indicates their association in apatite. Fe_2O_3 contents range from 6.08–10.42% and show a very high correlation with Al_2O_3 (r = 0.96), while TiO_2 and K_2O contents show little variation (0.50–0.93%, 1.70–3.34% respectively) and a very high correlation with Al_2O_3 (r = 0.99 for both elements), indicating an interdependence with terrigenous material. MgO contents range from 1.63 to 2.45%, while SO_3 contents vary from 0.20 to 0.59%. MnO contents vary from 0.05 to 0.20%.

The calcareous concretions group is characterized by the predominance of CaO and SiO_2; Al_2O_3, Fe_2O_3, MnO and MgO are the next abundant elements, while concentrations of all other oxides [K_2O, TiO_2 and SO_3] are lower than 1%. The major element composition reflects the dominance of calcite as the primary mineral in the calcareous concretions with subordinate quartz and clay minerals (Fig. 7B). CaO contents vary from 37.56 to 46.85%. MgO contents range from 1.36 to 1.69%. SiO_2 and Al_2O_3 concentrations show moderate variation (12.7–24.12%, 3.41–7.26% respectively), that reflects the variable proportions of quartz and mixed clay assemblages (Fig. 7A). Fe_2O_3 and K_2O concentrations show little variation (2.17–3.45, 0.59–1.27% respectively). TiO_2 contents vary from 0.19 to 0.41%. SiO_2, Fe_2O_3, K_2O and TiO_2 show a linear correlation with Al_2O_3 (r = 0.99 for all the mentioned elements), indicating their association with terrigenous material. The SO_3 contents range from 0.17 to 0.26%. The very high correlation with Fe_2O_3 (r = 0.99) and Zn (r = 0.71) highlights the presence of sulphides (sphalerite, pyrite) in the samples. P_2O_5 contents vary between 0.14 and 0.41%. A peculiarity of the calcareous concretions is their MnO-enriched concentrations (1.56–1.87%) compared to all the other samples (average value of 0.29%). This suggests the presence of rhodocrosite or manganocalcite in the composition of the calcareous concretions.

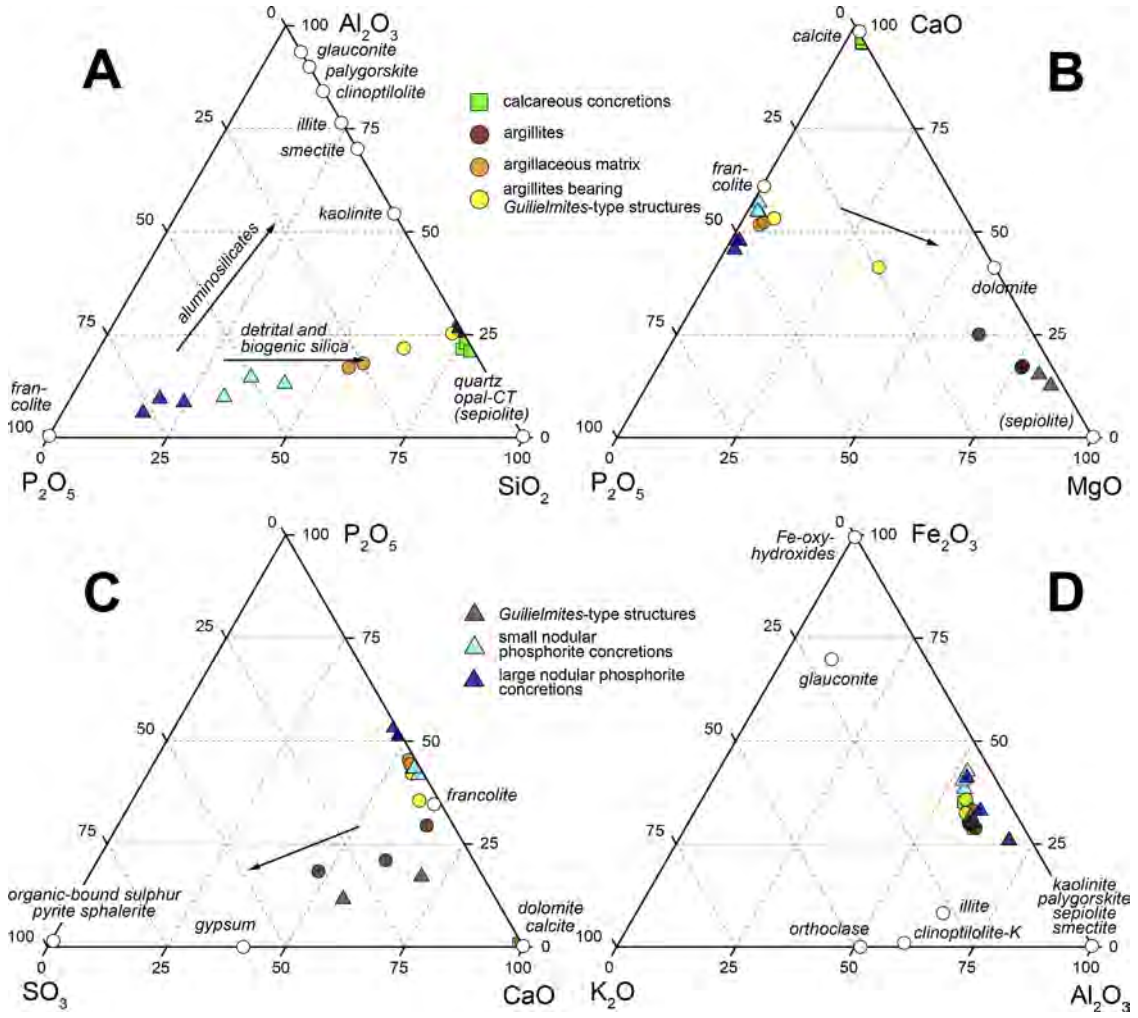

Fig. 7. Ternary diagrams illustrating selected major oxide variation in the lithologies of the Kalyus Beds. Numerical data are represented in Table 1. Stoichiometric compositions of the main mineral phases identified by light microscopy and x-ray diffraction studies are shown for comparison (modified from Garnit et al., 2017).

4.3. Trace elements

The abundance of trace elements (in ppm) is listed in Table 2. Th and Sc concentrations have values within the range of 0.8–35.2 ppm and 3.3–68.6 ppm, respectively. The variation ranges of Th/Sc and Cr/Th ratios are 0.25–1.05 and 0.84–7.93, respectively. Other parameters such as Th/V, Zr/V, Th/Ni and Zr/Ni have values within the range of 0.05–0.38, 0.56–1.23, 0.06–0.84 and 0.45–4.02, respectively.

Sr is an element that readily substitutes for Ca in francolite (Jarvis et al., 1994) and is enriched (> 400 ppm) in the phosphorites and enriched argillites groups. High contents of Zn and Cu (> 100 ppm) in the lithologies of the phosphorites group point out the presence of sphalerite and chalcopyrite mineral phases. Overall, the highest contents in trace elements are in the samples of the pure argillites and enriched argillites groups, except for Cu and Zn which exhibits the highest contents in the phosphorites group.

The enrichment or depletion of trace elements in all samples compared with the mean compositions of the upper continental crust (UCC) of Taylor and McLennan (1985) is shown in Fig. 8. The pure argillites group almost always shows values of trace elements close to the UCC ratio. The phosphorites group shows relative authigenic enrichment in Mo, U, Ni, Cu, and no enrichment in V and Cr. The carbonates group exhibits relative authigenic enrichment in Mo, U, Ni and no enrichment in V, Cr, Cu. The enriched argillites show no enrichment in Cr, Cu, Ni, V, U, and Mo and indicate values close to the UCC ratio. Although the enriched argillites group have high ΣREE and MREE/MREE* values, they show nearly the same contents of all the trace elements (except of Sr) as the pure argillites group. On the other hand, carbonates are enriched in such elements as Mo, Sb, Ni and Sr compared to the pure argillites, but at the same time have low ΣREE and MREE/MREE* values. The phosphorites group compared to the pure argillites indicates relative authigenic enrichment in more trace elements, such as Mo, Cu, Zn, Ge, Ni, Ba and Sr.

4.4. REE data

The results of the geochemical analyses (REE data) are listed in Table 3 and calculated values of geochemical parameters in Table 4. Total REE concentrations (ΣREE) in the analysed samples range between 72 and 1735 ppm. The concentrations of ΣREE show significant differences amongst the different lithological types.

The phosphorites group shows strong MREE-enriched patterns and is characterised by high ΣREE (1169–1533 ppm), high MREE/MREE* (6.39–7.95), low Ce/Ce* (0.58–0.92), high Eu/Eu* (1.02–1.58). The carbonates group exhibits LREE-depleted patterns with low ΣREE (72–125 ppm), low MREE/MREE* (1.62–1.84), high Ce/Ce* (0.80–1.02), moderate Eu/Eu* (0.93–0.95). The enriched argillites group indicates moderately MREE-enriched patterns with high ΣREE (793–1735 ppm), high MREE/MREE* (4.45–5.80), high Ce/Ce* (0.97–1.12), moderate Eu/Eu* (0.97–1.21). The pure argillites group shows nearly flat REE patterns, low ΣREE (199–296 ppm), low MREE/MREE* (1.02–1.63), moderate Ce/Ce* (0.90–0.91), and moderate Eu/

Table 2
Trace element contents in the Ediacaran Kalyus Beds, Naslavcea Quarry, Republic of Moldova (C – calcareous concretions; A – argillites; F – *Guilielmites*-type structure; M – argillaceous matrix; MF – argillites bearing *Guilielmites*-type structures; PS – small nodular phosphorite concretions; PL – large nodular phosphorite concretions).

Sample	501 C	516 C	519 C	502 A	503 A	504 A	511 F	512 F	507 M	508 M	513 MF	515 MF	505 PS	506 PS	509 PS	517 PL	518 PL	401 PL
Sc	14.1	4.6	4.2	51.2	58.4	68.6	47.2	41.9	29.6	28.9	37.9	35.2	6.4	8.0	13.7	8.6	3.5	3.3
V	57.7	19.3	15.0	232.3	261.8	210.1	204.8	182.5	136.0	133.4	142.3	142.1	21.0	22.3	36.1	27.8	11.4	16.9
Cr	31.2	8.8	6.5	124.5	146.6	120.8	107.3	99.9	68.9	66.5	73.3	81.0	7.7	7.1	12.6	14.6	3.1	6.6
Co	10.3	2.7	3.6	42.6	22.4	37.0	24.1	25.3	13.5	14.4	23.0	21.1	3.0	2.8	5.6	4.0	1.9	2.5
Ni	25.0	13.0	12.9	60.9	56.3	62.5	56.6	56.2	41.6	40.8	42.6	36.8	25.8	24.8	25.2	18.6	16.8	14.1
Cu	6.1	2.9	1.9	26.1	31.4	40.9	25.1	28.3	14.7	14.7	18.4	18.4	156.6	129.0	9.5	248.0	69.6	8.7
Zn	19.2	21.6	4.8	81.8	118.1	110.2	73.0	66.9	47.5	43.2	48.5	54.8	531.0	86.3	9.7	10.9	19.9	11.4
Ga	6.8	2.1	1.7	29.7	34.8	38.3	28.2	26.2	17.6	17.3	19.6	22.5	3.5	3.7	5.0	4.1	2.5	2.4
Rb	212	69	55	631	759	852	688	629	365	505	421	531	56	56	95	92	25	11
Sr	176	155	150	142	122	129	109	101	671	563	387	190	492	562	558	375	366	254
Zr	61.7	17.8	14.2	192.5	181.0	194.3	185.0	170.1	121.6	116.8	122.0	147.8	11.7	18.7	35.1	34.1	10.0	12.8
Nb	5.4	1.7	1.5	20.3	22.4	16.6	19.2	16.8	8.7	13.1	9.5	13.1	1.0	1.1	2.4	2.5	0.8	1.4
Mo	1.1	1.1	0.8	0.9	0.9	1.3	1.0	0.9	0.7	0.8	0.6	0.7	0.6	0.4	0.4	0.9	0.4	0.4
Ag	0.1	0.0	0.0	0.2	0.2	0.2	0.2	0.2	0.1	0.1	0.2	0.2	0.0	0.0	0.0	0.0	0.0	0.0
Cd	0.0	0.0	0.0	0.0	0.0	0.0	0.0	0.0	0.0	0.0	0.0	0.0	0.6	0.0	0.0	0.0	0.0	0.0
Sn	0.7	0.3	0.2	3.2	3.7	3.9	3.7	3.3	2.0	2.3	2.6	3.1	0.4	0.5	0.5	0.6	0.2	0.8
Sb	0.1	0.0	0.1	0.2	0.1	0.2	0.2	0.2	0.2	0.2	0.2	0.1	0.0	0.0	0.1	0.0	0.0	0.0
Cs	19.5	7.4	5.7	79.4	93.5	112.3	96.4	89.0	45.2	43.6	52.5	79.0	4.4	4.6	7.6	7.7	2.2	0.4
Ba	184.7	69.2	69.8	726.8	609.1	616.5	546.5	566.6	573.5	708.9	585.5	582.0	189.3	246.8	367.7	267.4	327.5	91.0
Hf	1.1	0.4	0.3	4.8	4.2	4.6	5.3	4.9	3.3	3.3	3.4	3.4	0.5	0.7	1.0	1.0	0.7	0.6
W	0.6	0.3	0.2	1.8	1.8	1.6	1.9	1.6	1.4	1.6	1.9	1.4	0.6	0.9	1.1	0.7	0.6	0.7
Pb	6.9	4.9	5.4	17.0	16.8	20.0	22.9	22.0	12.5	14.9	13.9	13.6	3.4	6.9	6.4	19.3	15.6	2.2
Th	7.3	1.9	2.0	29.4	30.7	34.8	35.2	32.4	22.4	21.7	21.9	30.9	3.3	8.4	4.1	6.2	1.4	0.8
U	0.9	0.4	0.3	3.4	4.6	4.5	3.5	3.0	4.8	4.5	6.9	5.0	0.6	0.7	2.1	1.2	0.8	0.8

Eu* (0.94–0.97). The variation ranges of $(La/Sm)_N$, $(La/Yb)_N$ and Y/Ho ratios are 0.03–1.48, 0.24–1.30 and 25.6–52.5, respectively.

The contribution of siliciclastic material to the ΣREE in different lithological types from the Kalyus Beds was investigated using plots of Y/Ho versus ΣREE, MREE/MREE*, Ce/Ce* or Eu/Eu* (Figs. 9 and 10). Greater terrigenous influence should result in shifts toward lower Y/Ho (~25–30) and higher ΣREE or MREE/MREE*, while seawater influence exhibits variable Y/Ho ratios but about as twice as that of terrigenous siliciclastics, commonly ~60, low ΣREE and LREE depletion (Kamber and Webb, 2001). We show that there are four discrete sample groups with variable ratios between hydrogenous and terrigenous components – phosphorites, carbonates, enriched argillites and pure argillites. The enriched argillites group plots closer to the phosphorites group and the pure argillites group plots closer to the carbonates group.

The total REEs content in the small and large phosphorite concretions is much higher than the mean values (457 ppm) in apatite crystals of phosphorites (Table 3, and Altschuler, 1980). For the argillites, argillaceous matrices and argillites from the layers bearing *Guilielmites*-type structures, the total concentrations of REEs are much higher than the average concentration (185 ppm) of PAAS (Taylor and McLennan, 1985).

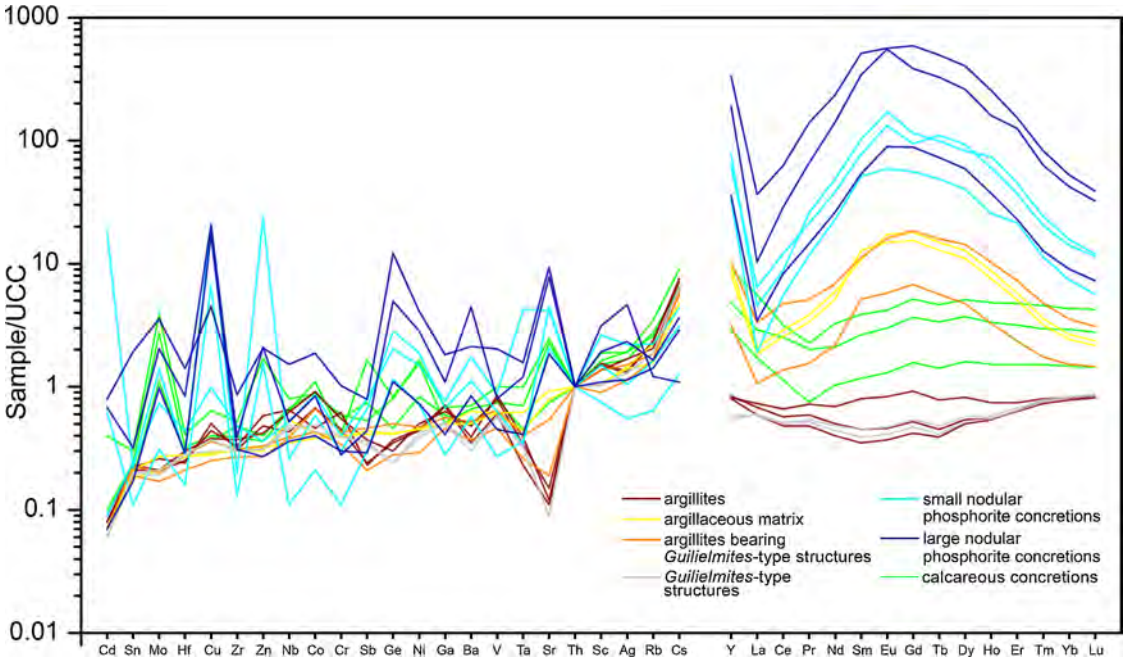

Fig. 8. UCC-normalized trace elements and REEs spidergram distributions for the samples from the Kalyus Beds, Nagoryany Formation.

Table 3
REE contents in the Ediacaran Kalyus Beds, Naslavcea quarry, Republic of Moldova (C – calcareous concretions; A – argillites; F – *Guilielmites*-type structures; M – argillaceous matrix; MF – argillites bearing *Guilielmites*-type structures; PS – small nodular phosphorite concretions; PL – large nodular phosphorite concretions).

Sample	501 C	516 C	519 C	502 A	503 A	504 A	511 F	512 F	507 M	508 M	513 MF	515 MF	505 PS	506 PS	509 PS	517 PL	518 PL	401 PL
Y	43.42	34.97	20.09	48.39	51.12	60.08	39.42	38.47	429.59	364.01	464.65	200.89	531.49	571.13	518.28	452.88	560.07	567.64
La	35.41	30.15	16.61	48.62	63.16	65.88	59.18	53.83	131.56	112.71	204.29	92.88	42.50	44.65	73.68	59.52	41.52	85.34
Ce	49.20	36.28	30.72	85.07	121.32	118.27	108.38	97.04	385.54	331.99	619.66	253.92	174.69	276.99	293.97	307.31	246.71	312.21
Pr	3.64	2.89	2.74	9.39	14.65	13.49	12.58	11.07	56.80	48.22	74.30	31.73	57.18	65.14	57.58	59.78	62.59	77.16
Nd	18.26	15.21	10.42	28.83	51.77	42.42	40.99	34.74	321.78	271.03	365.47	163.84	394.43	467.05	380.03	395.45	492.05	475.83
Sm	3.58	3.12	2.27	4.31	10.32	6.59	6.74	5.29	100.68	116.80	102.62	67.00	143.32	180.49	133.38	139.87	206.00	179.26
Eu	0.78	0.66	0.50	0.90	2.09	1.31	1.37	1.09	31.83	26.66	28.93	14.67	46.92	40.64	44.45	45.47	65.07	38.55
Gd	4.05	3.51	2.65	4.43	10.00	6.48	6.75	5.39	141.85	118.85	143.87	74.39	135.76	166.33	136.60	194.36	195.63	174.57
Tb	0.62	0.53	0.41	0.68	1.43	0.94	1.00	0.80	19.90	16.73	20.86	10.41	19.76	24.45	27.00	26.96	28.08	24.70
Dy	3.81	3.21	2.47	4.84	8.20	6.11	6.55	5.50	93.44	78.50	102.80	47.86	89.55	110.34	124.02	119.72	122.19	110.14
Ho	0.83	0.69	0.51	1.20	1.70	1.43	1.54	1.34	14.62	12.27	16.81	7.53	18.41	16.02	18.29	17.23	17.10	15.91
Er	2.38	1.96	1.39	4.05	4.89	4.69	5.06	4.48	27.87	23.66	34.30	15.61	32.28	38.70	32.40	30.52	38.75	27.52
Tm	0.34	0.27	0.19	0.70	0.75	0.78	0.85	0.76	2.47	2.13	3.24	1.66	2.48	2.93	2.57	2.43	2.79	2.12
Yb	2.21	1.70	1.23	4.99	5.11	5.56	6.02	5.43	12.22	10.82	15.97	9.68	10.76	12.73	11.83	11.52	12.48	9.02
Lu	0.31	0.24	0.17	0.76	0.77	0.84	0.91	0.82	1.58	1.40	2.03	1.35	1.19	1.41	1.40	1.35	1.38	0.97
ΣREE	125	100	72	199	296	275	258	228	1342	1172	1735	793	1169	1448	1337	1411	1532	1533
Ce/Ce*	0.91	0.80	1.02	0.90	0.91	0.90	0.90	0.90	0.97	0.98	1.12	1.05	0.58	0.81	0.87	0.92	0.76	0.71
Eu/Eu*	0.95	0.93	0.95	0.97	0.97	0.94	0.95	0.96	1.21	1.06	1.08	0.97	1.58	1.10	1.54	1.26	1.52	1.02

Table 4
REE contents and compositions for each group of the Kalyus Beds.

	phosphorites group	enriched argillites group	pure argillites group	carbonates group
ΣREE (ppm)	1169–1533	793–1735	199–296	72–125
$(La/Sm)_N$	0.03–0.08	0.14–0.30	0.92–1.69	1.10–1.48
$(La/Yb)_N$	0.24–0.69	0.70–0.94	0.71–0.91	0.99–1.30
$(Sm/Yb)_N$	5.93–9.71	3.14–5.28	0.42–0.99	0.79–0.90
MREE/MREE*	6.39–7.95	4.45–5.80	1.02–1.63	1.62–1.84
Y/Ho	26.3–35.7	26.7–29.7	25.6–40.4	39.5–52.5
Ce/Ce*	0.58–0.92	0.97–1.12	0.90–0.91	0.80–1.02
Eu/Eu*	1.02–1.58	0.97–1.21	0.94–0.97	0.93–0.95

5. Discussion

5.1. Lithogenous versus hydrogenous REE sources

Certain lithological types can record a hydrogenous, lithogenous or mixed signature (Zhao et al., 2013; Chen et al., 2015; Zhang et al., 2016). The use of the Y/Ho proxy may help in the evaluation of the hydrogenous versus lithogenous contribution to ΣREE (e.g. Zhang et al., 1994; Nozaki et al., 1997).

The phosphorites and enriched argillites group show signatures of predominant terrigenous origin (Figs. 9 and 10). In these conditions, most REEs are derived from argillites of the host rock, but have been reprocessed through absorption/desorption reactions into Fe-oxyhydroxides before final uptake of the phosphate. These diagenetic processes led to the characteristic hat-shaped MREE-enriched pattern. Since these lithologies did not preserve a hydrogenous signature, the Ce/Ce* and Eu/Eu* anomalies cannot be used for interpretations of the depositional environment (e.g. Chen et al., 2015; Zhang et al., 2016). The pure argillites group has a flat distribution pattern that closely matches that of UCC (Taylor and McLennan, 1985). These samples preserve a terrigenous signal, although with some hydrogenous influence, which means that the REE composition of pure argillites is not suitable for the purpose of paleomarine environmental reconstruction.

The calcareous concretions are diagenetic structures, but lack evidence for REE enrichment processes. The relatively high Y/Ho ratios as well as a flat distribution pattern suggest that these samples preserved a hydrogenous signal, but with some minor lithogenous influence. These samples show distinct features that provide insight into the nature of the early diagenetic conditions under which they formed. Therefore, this is the only sample group from the four groups for which the Ce and Eu anomalies can be meaningfully interpreted. The Eu/Eu* values are an indication of REE inputs from mixed sources, but with a predominant influx of felsic minerals that precipitate from late stage, Eu-depleted magmas (Chen et al., 2015). In addition, the sulphides found in phosphorite and calcareous concretions may be of primary authigenic origin.

5.2. Source area

Moderate concentrations of Rb (> 55 ppm) in the phosphorites and carbonates groups indicate incorporation of clay minerals from the host rocks during the formation of the phosphorites and calcareous concretions. High concentrations of Rb (> 450 ppm) for the pure argillites and enriched argillites suggest the presence of clay minerals and a possible granitic source, especially kaolinized intrusives (e.g. Kostitsyn et al., 2007), whereas higher concentrations of V (> 100 ppm), Ni (> 40 ppm), Cr (> 70 ppm), Co (> 15 ppm) than in granites (e.g. Kostitsyn et al., 2007) and slightly lower concentrations than those in basalts (e.g. Nosova et al., 2008; Shumlyanskyy, 2012) indicates that a basaltic source has played a role in the sedimentation process.

The Th/Sc ratios are very useful in distinguishing between felsic and mafic provenances (e.g. McLennan et al., 1980). These ratios are unaffected by sedimentary processes, thus Th can be used as an indicator of a felsic source, while Sc can be used as an indicator of a mafic source (Taylor and McLennan, 1985). The Th versus Sc plot (Fig. 11), adopted from McLennan et al. (1993) reveals two source areas, a predominant intermediate source for most lithologies and a subordinate mafic source for the pure argillites group, respectively.

The possibility of the heavy mineral enrichment was explored by using Th/V vs. Zr/V and Th/Ni vs. Zr/Ni ratios, which are good overall indicators of igneous chemical differentiation processes (Hiscott, 1984; Taylor and McLennan, 1985; McLennan, 2001). The Th/V vs. Zr/V diagram points out that the obtained data do not intersect a primary compositional trend (Fig. 12A, dashed line), but plot near the granodiorite value as well as the average value of the PAAS and UCC. At the same time, the Th/Ni vs. Zr/Ni diagram (Fig. 12B) indicates that the phosphorites and carbonates groups plot near mixed basalt-andesite values, while the enriched and pure argillites groups plot near the granodiorite value as well as the average value of the PAAS and UCC.

To better constrain the mafic versus felsic character of the terrigenous fraction, elemental ratios such as Cr/Th and Th/Sc were plotted (Fig. 13). High values of these ratios indicate enrichment in mafic and

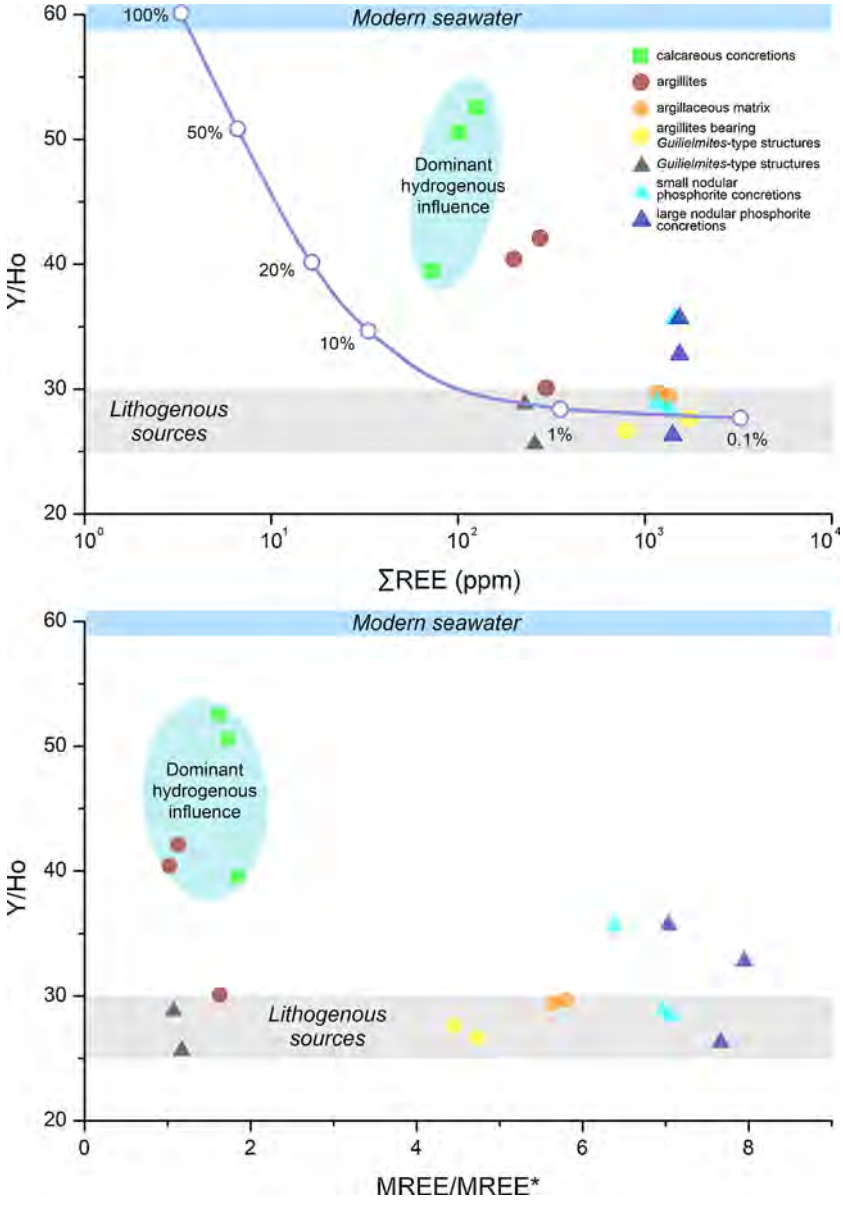

Fig. 9. (A) Y/Ho versus ΣREE, and (B) Y/Ho versus MREE/MREE* for the samples of the Kalyus Beds. The blue curve in A represents mixing between a hydrogenous component (Nozaki, 2001) and a terrigenous component with UCC composition (McLennan, 2001); percentages given as proportion of the hydrogenous component. (For interpretation of the references to colour in this figure legend, the reader is referred to the web version of this article).

felsic components, respectively (Hofmann et al., 2003; Bracciali et al., 2007). Studied samples plot near the felsic end member with a minor contribution from mafic sources (average values between 10–20%).

After the break-up of Rodinia, Baltica was an isolated continent (e.g. Cawood et al., 2001; Hartz and Torsvik, 2002; Shumlyanskyy et al., 2007; Li et al., 2013). Given its proximal location, the Archean-Paleoproterozoic Ukrainian Shield was an important supplier of terrigenous material for the Kalyus sedimentary basin, especially of felsic rocks which are found extensively throughout the Shield (e.g. Shumlyanskyy et al., 2018). At the same time, during the middle to late Ediacaran (590–560 Ma) (e.g. Shumlyanskyy et al., 2016) the proximal Volyn-Brest continental flood basalt province covered much of the area situated to the north of the Podolian basin. Borehole data (AGMR, 1994) combined with other studies (Srodon et al., 2019) indicates that our study area contains basalts and tuffs at the base of the Ediacaran succession. Consequently, mafic rocks from the Volyn-Brest continental flood basalt province played a role as a source of material during the sedimentation of the Kalyus Beds as well as for the other formations of the Ediacaran succession. Also, it is possible to assume that granites and gneisses from the Fennoscandian Shield (e.g. Johansson et al., 2016; Heinonen et al., 2010, 2015) were source rocks for the Kalyus Beds, but geochronological analyses on zircons are needed to confirm or deny this assumption.

5.3. MREE enrichment of phosphates during diagenesis

Phosphorites and enriched argillites show an MREE-enriched distribution pattern (Fig. 8) as seen in many paleomarine units (Lécuyer et al., 1998; Girard and Lécuyer, 2002; Bright et al., 2009; Chen et al., 2015; Zhang et al., 2016). However, the carbonates yielding a predominantly hydrogenous REE signature have a flat distribution pattern, so the MREE hat-shaped pattern is definitely not a primary feature. Further, it indicates that the MREE hat-shaped pattern was not acquired at the sediment-water interface during early diagenesis but, rather, at greater burial depths during late diagenesis.

Late diagenesis leads to the increase of the total REE content in

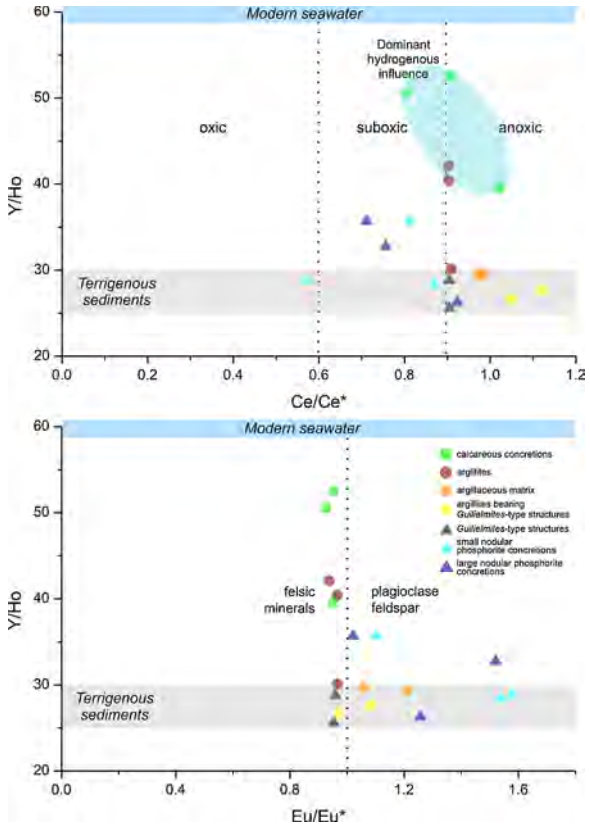

Fig. 10. (A) Y/Ho versus Ce/Ce*, and (B) Y/Ho versus Eu/Eu* for the lithological types of the Kalyus Beds (modified from Chen et al., 2015).

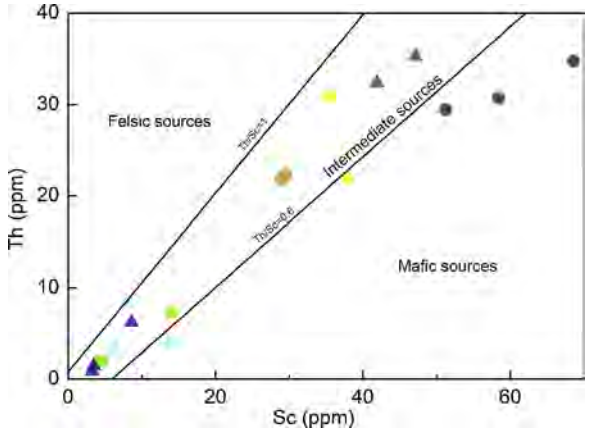

Fig. 11. Th versus Sc diagram indicating felsic and mafic provenance for the lithologies of the Kalyus Beds.

phosphorites and enriched argillites. Increased ΣREE is associated with lower Y/Ho ratios, indicating that diagenetic addition of REEs is correlated with their release from lithogenous materials, probably land-derived clay minerals and heavy minerals. The characteristics of the pure argillites group point out a lithogenous geochemical signature, but without REE or trace element enrichment. Most probably, the absorption/desorption processes during late diagenesis released REEs in the case of the pure argillites, meanwhile the phosphorites and enriched argillites accumulated REEs. The sequestration has an affinity towards phosphate minerals, as results show that the lithological types which contain apatite have increased ΣREE contents (Fig. 14), while lithological types with insignificant contents of apatite show low ΣREE contents with a flat-line distribution. At the same time, the samples from the carbonates group preserve a dominant early diagenetic signature, indicating minimal later-stage burial alteration and no MREE enrichment. Thus, the primary contribution of REEs in the Kalyus Beds is attributed to the phosphorus-enriched terrigenous material derived from the weathering and erosion of felsic and mafic rocks of the Ukrainian Shield and Volyn-Brest continental flood basalt province, while the secondary input of REEs is due to diagenesis.

Evidence for post-depositional uptake of REEs in the analysed lithologies was assessed by using a plot of $(La/Yb)_N$ versus $(La/Sm)_N$ which is used to check the effects of early to late diagenesis and also the possible substitutions in samples compared to modern seawater (Reynard et al., 1999). The values of $(La/Sm)_N$ in the phosphorites and enriched argillites groups show values that plot precisely on the late diagenesis (recrystallization) trend line (Fig. 15), which once again validates the fact that MREE-enriched patterns were obtained due to the strong influence of diagenetic fluids which have modified the composition and distribution of REEs in the previously mentioned rock types. In the case of pure argillites and carbonates, the $(La/Sm)_N$ ratios have a range which is comparable with the corresponding values of modern seawaters (0.79–1.66; Reynard et al., 1999). On the other hand, the values of $(La/Yb)_N$ in the mentioned samples show values which are greater than the corresponding values of the modern seawaters (0.20–0.50; Reynard et al., 1999). Knowing that the REE models of these two lithologies show shale-type patterns, with insignificant MREE enrichment it can be assumed that: (1) absorption processes of REEs took place during early diagenesis in interaction with the detrital siliciclastic material rich in REE; (2) the features of pure argillites and carbonates groups emphasize the composition of the Ediacaran seawater, which was different from that of the modern seawater.

Many authors consider that the hat-shaped MREE-enriched pattern which is common in phosphorites is the result of long-term diagenetic enrichment (McArthur and Walsh, 1984; Chen et al., 2015). Studies of Ediacaran (Felitsyn and Morad, 2002; Xin et al., 2016) and Cambrian (Mazumdara et al., 1999; Jiang et al., 2007; Zhu et al., 2014) sedimentary deposits have documented MREE enrichment of the phosphorites and phosphatic rocks. In all of these cases, MREE is a secondary feature associated with diagenetic enrichment of REEs.

5.4. Oceanic redox conditions

Cerium (Ce) is the only REE that is influenced by redox processes in the Earth-surface environment (Jarvis et al., 1994; Zhao et al., 2013). If a sample contains hydrogenously sourced Ce, then the Ce anomaly can be used as a seawater paleoredox proxy or as an indicator of adsorption/desorption processes (Wright et al., 1987; Holser, 1997). Contrarily, if Ce is primarily of terrigenous origin, then it is an indicator of sediment provenance. In the study section the calcareous concretions are the only group which retained a hydrogenous signature, therefore Ce was probably derived from the seawater and taken during early diagenesis, as were the other REEs (see Section 5.1). In this case, the REE composition of calcareous concretions is suitable for the purpose of paleomarine environmental reconstruction. The observed Ce/Ce* ratios are indicative of a suboxic to anoxic depositional environment (Fig. 10).

There is no evidence for continuous and large-scale anoxia along the shallow continental margins of Baltica during the late Ediacaran (Johnston et al., 2012). However, our current results show that during the sedimentation of the Kalyus Beds locally developed suboxic to anoxic conditions were prevalent. Contemporary anoxic events in the western margin of Baltica (Meinhold et al., 2019), South China (Wang et al., 2016; Zhang et al., 2018), Namibia (Wood et al., 2015) suggest that marine anoxia may have been more than a locally constrained phenomenon during the late Ediacaran, specifically from 551 to 541 Ma. These conditions may have contributed to the decline of the famous Ediacaran fauna, since these organisms thrived in predominantly oxic conditions.

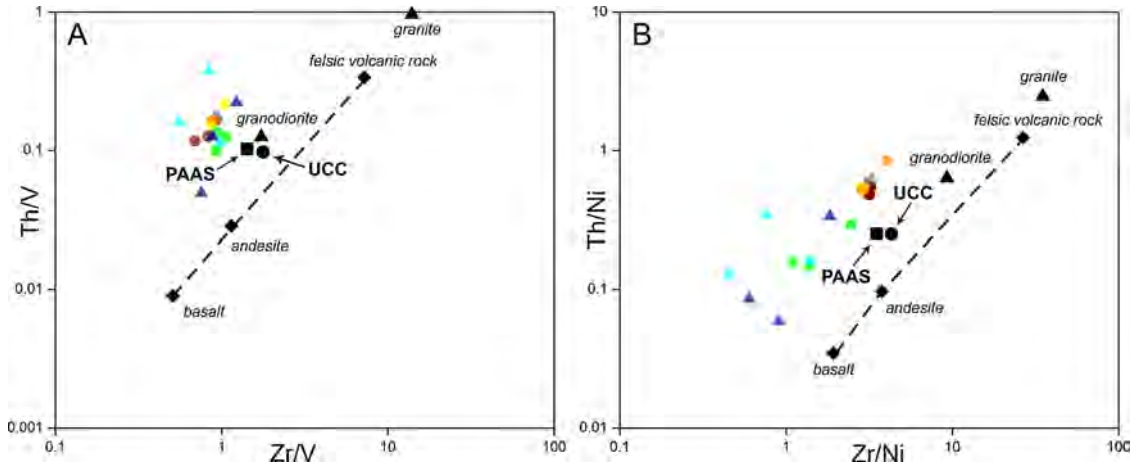

Fig. 12. Plots of Th/V vs. Zr/V (A), and Th/Ni vs. Zr/Ni (B), comparing the studied samples and post-Archean Australian average shale (PAAS; Taylor and McLennan, 1985; McLennan, 2001), Upper Continental Crust (UCC; Taylor and McLennan, 1985). Igneous rock compositions are average values from Condie (1993).

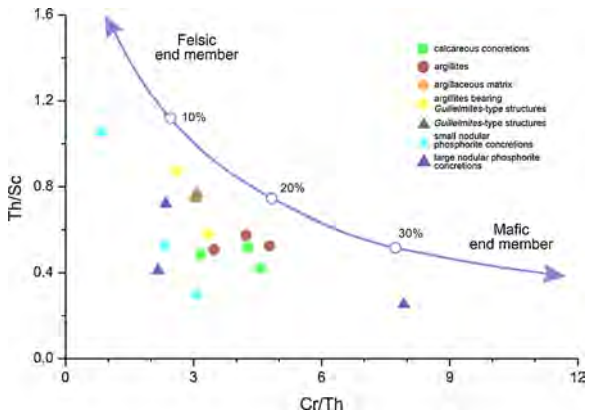

Fig. 13. Plot of Th/Sc versus Cr/Th (modified after Condie and Wronkiewicz, 1990) for the lithological types of the Kalyus Beds. All samples are consistent with a felsic end member with influences of a mafic end member.

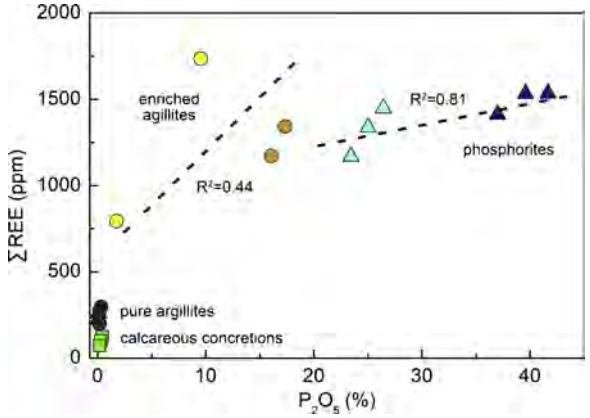

Fig. 14. Bivariate plot of total rare-earth elements (ΣREE, ppm) versus P_2O_5 (wt %) contents in the lithologies of the Kalyus Beds.

5.5. Economic value

As the demand for REEs increases each year, so does the annual world production of total rare earth oxides (Christmann, 2014). The overall ΣREE contents of the Kaylus Beds are high (793–1735 ppm) with a particular enrichment of MREE, and could be of potential economic interest. The phosphorites group of the Kalyus Beds are highly REE enriched, similar to several phosphorite deposits of the world (Fig. 16).

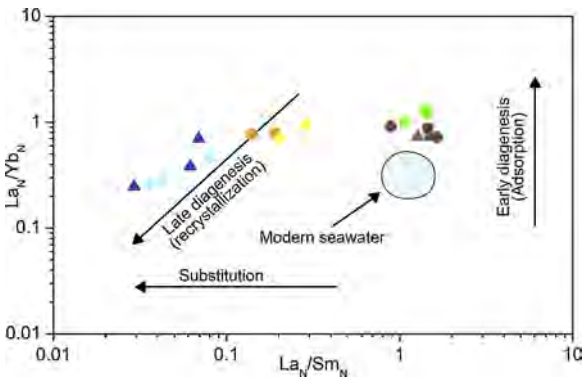

Fig. 15. $(La/Yb)_N$ vs $(La/Sm)_N$ plots (modified after Reynard et al., 1999). Small and large nodular phosphorite concretions, argillaceous matrices, argillites bearing *Guilielmites*-type structures fall into the late diagenesis field.

The Kalyus Beds occur extensively along the middle course of the Dniester River basin (Fig. 17), with outcrops on the territories of Moldova and Ukraine (Bukatchuk, 1973; Velikanov et al., 1983). Compared to the other formations of the Ediacaran succession, the Kalyus Beds are laterally consistent, show minor facies variations, have a constant general thickness of 20–45 m (e.g. Velikanov et al., 1983; Sokur and Figura, 2009), and commonly contain nodular phosphorite concretions.

6. Conclusions

Two types of REE patterns have been distinguished in the late Ediacaran Kalyus Beds from the southwestern part of the East European Platform. Flat distribution patterns are characteristic to the pure argillites and calcareous concretions. Middle-REE enriched patterns are common in both phosphorites and enriched argillites. There is a direct relationship between phosphorus concentrations and REE abundances in the enriched argillites and phosphorites groups. Thus, REE variation appears to be controlled by apatite content. This was possible due to the primary input of land-derived terrigenous material as well as secondary enrichment during late diagenesis. Baltica was a separate continent throughout the late Ediacaran, therefore sources of terrigenous material were presumably the felsic rocks of the Ukrainian Shield and the mafic rocks of the Volyn-Brest continental flood basalt province. Although there is evidence for persistent and extensive oxic conditions on and around the shallow continental margins of Baltica during the late Ediacaran, our investigations suggest that the sedimentation of the Kalyus Beds was a temporal and local episode of anoxia. The correlation with other anoxic events during the late Ediacaran merits further consideration.

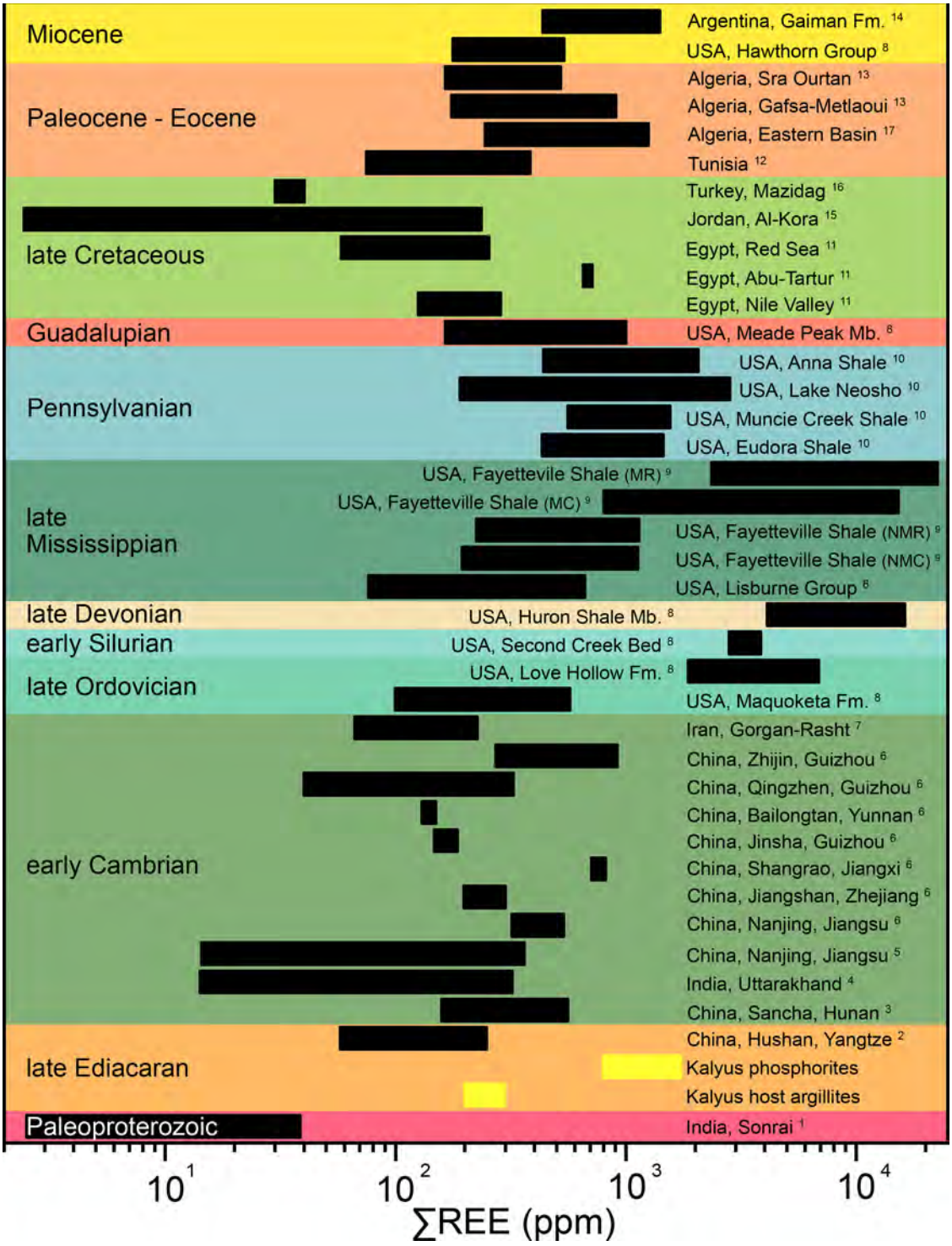

Fig. 16. Comparison of total REE contents between several sedimentary phosphorite deposits, based on geological age and location. Data from 1. Khan et al., 2012; 2. Xin et al., 2016; 3. Zhu et al., 2014; 4. Khan et al., 2016; 5. Jiang et al., 2007; 6. Chen et al., 2013; 7. Abedini and Calagari, 2017; 8. Emsbo et al., 2015; 9. Murthy et al., 2004; 10. Kidder and Eddy-Dillek, 1994; 11. Baioumy, 2011; 12. Garnit et al., 2012; 13. Kechiched et al., 2016; 14. Fazio et al., 2007; 15. Abed et al., 2016; 16. Öztürk et al., 2019; 17. Garnit et al., 2017. NMC – non-marine core; NMR – non-marine rim; MC – marine core; MR – marine rim.

Also, additional investigations are needed to establish some economically feasible areas for open-pit exploitation. Our preliminary results show that the ΣREE concentrations of phosphorites and enriched argillites groups (793–1735 ppm) are high compared to several other phosphorite deposits of the world. Although the host rock has lower ΣREE contents (198–296 ppm), it should be taken into account that a whole-rock open-pit exploitation procedure might be economically feasible.

Declaration of Competing Interest

The authors declare that they have no known competing financial interests or personal relationships that could have appeared to influence the work reported in this paper.

Fig. 17. Approximative regional extension of outcrops of the Kalyus Beds (Ukrainian data from Velikanov et al., 1983; Moldavian data from the authors).

Acknowledgements

The authors gratefully acknowledge the constructive and thorough peer-reviewing of Stephen Kershaw (Brunel University, London), Sören Jensen (Universidad de Extremadura, Badajoz) and Guido Meinhold (Keele University). Thomas J. Algeo (University of Cincinnati) and Octavian G. Duliu (University of Bucharest) are kindly thanked for their suggestions and improvements on the early versions of the manuscript. Andrei Nosatii (Alexandru Ioan Cuza University, Iași) is warmly thanked for permission to use the SEM images of calcareous concretions. Valentin Paraschiv (Geological Institute of Romania) is thanked for his support during the field works. We are extremely grateful to the two anonymous reviewers, and also to Carita Augustsson, Handling Editor, and Astrid Holzheid, Editor-in-Chief, for the thoughtful reviewing and valuable comments and suggestions that essentially contributed to the improvement of our paper. We are thankful to Keerthika Maddala, Journal Manager, for the outstanding cooperation during the revision of proofs. This study was financially supported by the Romanian Executive Agency for Higher Education, Research, Development and Innovation Funding projectPN-II-RU-TE-2014-4-2064 to R.-D.R. and project PN-III-P4-ID-PCCF-2016-0014 to M.N.D.

References

Abed, A.M., Jaber, O., Alkuisi, M., Sadaqah, R., 2016. Rare earth elements and uranium geochemistry in the Al-Kora phosphorite province, Late Cretaceous, northwestern Jordan. Arab. J. Geosci. 9, 1–19. https://doi.org/10.1007/s12517-015-2135-6.

Abedini, A., Calagari, A.A., 2015. Rare earth element geochemistry of the Upper Permian limestone: the Kanigorgeh mining district, NW Iran. Turk. J. Earth Sci. 24, 365–382. https://doi.org/10.3906/yer-1412-30.

Abedini, A., Calagari, A.A., 2017. REEs geochemical characteristics of lower Cambrian phosphatic rocks in the Gorgan-Rasht Zone, northern Iran: implications for diagenetic effects and depositional conditions. J. Afr. Earth Sci. 135, 115–124. https://doi.org/10.1016/j.jafrearsci.2017.08.018.

Abedini, A., Calagari, A.A., Akbari, M., 2011. Geochemistry and genesis of Mehredjan bentonite deposit, southeast of Khoor, Isfehan province. J. Geopersia 1, 47–58. https://doi.org/10.22059/JGEOPE.2011.22164.

Agency of Geology and Mineral Resources (AGMR) of the Republic of Moldova, 1994. Geological Survey Report of the M-35 Topographic Map. pp. 1–443.

Algeo, T.J., Maynard, J., 2004. Trace-element behavior and redox facies in core shales of Upper Pennsylvanian Kansas-type cyclothems. Chem. Geol. 206, 289–318. https://doi.org/10.1016/j.chemgeo.2003.12.009.

Altschuler, Z.S., 1980. The geochemistry of trace elements in marine phosphorites part I. Characteristic abundance and enrichment. In: Bentor, Y.K. (Ed.), Marine Phosphorites, pp. 19–30 SPEM Special Publication 29.

Aseeva, E.A., 1976. Microphitofossils and algae from the Upper Precambrian deposits of Volyno-Podolia. In: Rjabenko, V.A., Velikanov, V.A., Aseeva, E.A., Palij, V.M., Tzegeliniuk, P.D., Zernetzkaja, N.V. (Eds.), Paleontology and Stratigraphy of the Upper Precambrian and Lower Paleozoic from the south-western part of the East-European Platform. Naukova Dumka, Kiev, pp. 40–63 (in Russian).

Baioumy, H., 2011. Rare earth elements and sulfur and strontium isotopes of upper Cretaceous phosphorites in Egypt. Cretac. Res. 32, 368–377. https://doi.org/10.1016/j.cretres.2011.01.008.

Bau, M., Dulski, P., 1996. Distribution of yttrium and rare-earth elements in the Penge and Kuruman iron-formations, Transvaal Supergroup, South Africa. Precambrian Res. 79, 37–55. https://doi.org/10.1016/0301-9268(95)00087-9.

Bracciali, L., Marroni, M., Pandolfi, L., Rocchi, S., 2007. Geochemistry and petrography of Western Tethys Cretaceous sedimentary covers (Corsica and Northern Apennines): from source areas to configuration of margins. Geol. Soc. Am. Spec. Pap. 420, 73–93. https://doi.org/10.1130/2006.2420(06).

Bright, C.A., Cruse, A.M., Lyons, T.W., MacLeod, K.G., Glascock, M.D., Ethington, R.L., 2009. Seawater rare earth element patterns preserved in apatite of Pennsylvanian conodonts? Geochim. Cosmochim. Acta 73, 1609–1624. https://doi.org/10.1016/j.gca.2008.12.014.

Bukatchuk, P.D., 1973. Upper Precambrian deposits from the southwestern part of the East-European Platform, Stratigraphy and Paleogeography (PhD Thesis). Moldovageology 1–272 (in Russian), Chisinau.

Bukatchuk, P.D., Bliuk, I.B., Pokatilov, V.P., 1988. Geological map of the Moldavian Soviet Socialist Republic, scale 1:200 000. Explanatory notes. Moldovageology 1–273 (in Russian), Chisinau.

Cawood, P.A., McCausland, P.J.A., Dunning, G.R., 2001. Opening Iapetus: constraints from the Laurentian margin in Newfoundland. Geol. Soc. Am. Bull. 113, 443–453. https://doi.org/10.1130/0016-7606(2001)113<0443:OICFTL>2.0.CO;2.

Chen, J., Yang, R., Wei, H., Gao, J., 2013. Rare earth element geochemistry of Cambrian phosphorites from the Yangtze Region. J. Rare Earths 31, 101–112. https://doi.org/10.1016/S1002-0721(12)60242-7.

Chen, J., Algeo, T.J., Zhao, L., Chen, Z.Q., Cao, L., Zhang, L., Li, Y., 2015. Diagenetic uptake of rare earth elements by bioapatite, with an example from Lower Triassic conodonts of South China. Earth Sci. Rev. 149, 181–202. https://doi.org/10.1016/j.earscirev.2015.01.013.

Christmann, P., 2014. A forward look into rare earth supply and demand: a role for sedimentary phosphate deposits? Procedia Eng. 83, 19–26. https://doi.org/10.1016/j.proeng.2014.09.005.

Condie, K.C., 1993. Chemical composition and evolution of the upper continental crust: contrasting results from surface samples and shales. Chem. Geol. 104, 1–37. https://doi.org/10.1016/0009-2541(93)90140-E.

Condie, K.C., 2001. Mantle Plumes and Their Record in Earth History. Cambridge University Press, Cambridge, pp. 1–306.

Condie, K.C., Wronkiewicz, D.J., 1990. The Cr/Th ratio in Precambrian pelites from the Kaapvaal craton as an index of craton evolution. Earth Planet. Sci. Lett. 97, 256–267. https://doi.org/10.1016/0012-821X(90)90046-Z.

Elderfield, H., 1988. The oceanic chemistry of the rare-earth elements. Philos. Trans.

Math. Phys. Eng. Sci. 325, 105–126. https://doi.org/10.1098/rsta.1988.0046.
Emsbo, P., McLaughlin, P.I., Breit, G.N., du Bray, E.A., Koenig, A.E., 2015. Rare earth elements in sedimentary phosphate deposits: solution to the global REE crisis? Gondwana Res. 27, 776–785. https://doi.org/10.1016/j.gr.2014.10.008.
Fazio, A.M., Scasso, R.A., Castro, L.N., Carey, S., 2007. Geochemistry of rare earth elements in early-diagenetic Miocene phosphatic concretions of Patagonia, Argentina: phosphogenetic implications. Deep Sea Res. II 54, 1414–1432. https://doi.org/10.1016/j.dsr2.2007.04.013.
Fedonkin, M.A., Gehling, J.G., Grey, K., Narbonne, G.M., Vickers-Rich, P., 2007. The Rise of Animals, Evolution and Diversification of the Kingdom Animalia. John Hopkins University Press, Baltimore, pp. 149–156.
Felitsyn, S., Morad, S., 2002. REE patterns in latest Neoproterozoic–early Cambrian phosphate concretions and associated organic matter. Chem. Geol. 187, 257–265. https://doi.org/10.1016/S0009-2541(02)00046-3.
Francovschi, I., Grădinaru, E., Roban, R.D., Ciobotaru, V., 2017. Subsurface data of the Ediacaran sedimentary series from the southwestern part of the East-European platform. SGEM 2017 Conference Proceedings 17, 549–556.
Garnit, H., Bouhlel, S., Barca, D., Chtara, C., 2012. Application of LA-ICP-MS to sedimentary phosphatic particles from Tunisian phosphorite deposits: insights from trace elements and REE into paleo-depositional environments. Chemie der Erde 72, 127–139. https://doi.org/10.1016/j.chemer.2012.02.001.
Garnit, H., Bouhlel, S., Jarvis, I., 2017. Geochemistry and depositional environments of Paleocene-Eocene phosphorites: Metlaoui Group, Tunisia. J. Afr. Earth Sci. 134, 704–736. https://doi.org/10.1016/j.jafrearsci.2017.07.021.
German, C.R., Elderfield, H., 1990. Application of the Ce anomaly as a paleoredox indicator: the ground rules. Paleoceanogr. Paleoclimatol. 5, 823–833. https://doi.org/10.1029/PA005i005p00823.
Girard, C., Lécuyer, C., 2002. Variations in Ce anomalies of conodonts through the Frasnian/Famennian boundary of Poland (Kowala Holy Cross Mountains): implications for the redox state of seawater and biodiversity. Palaeogeogr. Palaeoclimatol. Palaeoecol. 181, 299–311. https://doi.org/10.1016/S0031-0182(01)00482-5.
Gnilovskaya, M.B., Istchenko, A.A., Kolesnikov, C.M., Korenchuk, L.V., Udaltsov, A.P., 1988. Vendotaenids of the East European Platform. Nauka, Leningrad, pp. 1–143 (in Russian).
Goonan, T.G., 2011. Rare Earth Elements – End Use and Recyclability. U.S. Geological Survey Scientific Investigations Report 2011–5094. pp. 1–15. https://doi.org/10.3133/sir20115094.
Grazhdankin, D.V., Maslov, A.V., 2015. The room for the Vendian in the International Chronostratigraphic Chart. Russ. Geol. Geophys. 56, 549–559. https://doi.org/10.1016/j.rgg.2015.03.007.
Haley, B.A., Klinkhammer, G.P., McManus, J., 2004. Rare earth elements in pore waters of marine sediments. Geochim. Cosmochim. Acta 68, 1265–1279. https://doi.org/10.1016/j.gca.2003.09.012.
Hartz, E.H., Torsvik, T.H., 2002. Baltica upside down: a new plate tectonic model for Rodinia and the Iapetus ocean. Geology 30, 255–258. https://doi.org/10.1130/0091-7613(2002)030<0255:BUDANP>2.0.CO;2.
Heinonen, A.P., Andersen, T., Rämö, O.T., 2010. Re-evaluation of rapakivi petrogenesis: source constraints from the Hf isotope composition of zircon in the rapakivi granites and associated mafic rocks of southern Finland. J. Petrol. 51, 1687–1709. https://doi.org/10.1093/petrology/egq035.
Heinonen, A., Andersen, T., Rämö, O.T., Whitehouse, M., 2015. The source of Proterozoic anorthosite and rapakivi granite magmatism: evidence from combined in situ Hf–O isotopes of zircon in the Ahvenisto complex, southeastern Finland. J. Geol. Soc. 172, 103–112. https://doi.org/10.1144/jgs2014-013.
Hiscott, R.N., 1984. Ophiolitic source rocks for Taconic-age flysch: trace element evidence. GSA Bulletin 95, 1261–1267. https://doi.org/10.1130/0016-7606(1984)95<1261:OSRFTF>2.0.CO;2.
Hofmann, A., Bolhar, R., Dirks, P., Jelsma, H., 2003. The geochemistry of Archaean shales derived from a mafic volcanic sequence, Belingwe greenstone belt, Zimbabwe; provenance, source area unroofing and submarine versus subaerial weathering. Geochim. Cosmochim. Acta 67, 421–440. https://doi.org/10.1016/S0016-7037(02)01086-4.
Holser, W.T., 1997. Evaluation of the application of rare-earth elements to paleoceanography. Palaeogeogr. Palaeoclimatol. Palaeoecol. 132, 309–323. https://doi.org/10.1016/S0031-0182(97)00069-2.
Humphries, M., 2010. Rare earth elements: the global supply chain. CRS Report for Congress 1–27.
Ivantsov, A.Y., Gritsenko, V.P., Paliy, V.M., Velikanov, V.A., Konstantinenko, L.I., Menasova, A.S., Fedonkin, M.A., Zakrevskaya, M.A., Serezhnikova, E.A., 2015. Upper Vendian macrofossils of Eastern Europe. Middle Dniester area and Volhynia. PIN RAS, Moscow, pp. 1–144.
Jarvis, I., Burnett, W.C., Nathan, Y., Almbaydin, F.S.M., Attia, A.K.M., Castro, L.N., Flicoteaux, R., Hilmy, M.E., Husain, V., Qutawnah, A.A., Serjani, A., Zanin, Y.N., 1994. Phosphorite geochemistry: state-of-the-art and environmental concerns. Eclogae Geol. Helv. 87, 643–700.
Jiang, S.-Y., Zhao, H.-X., Chen, Y.-Q., Yang, T., Yang, J.-H., Ling, H.-F., 2007. Trace and rare earth element geochemistry of phosphate nodules from the lower Cambrian black shale sequence in the Mufu Mountain of Nanjing, Jiangsu province, China. Chem. Geol. 244, 584–604. https://doi.org/10.1016/j.chemgeo.2007.07.010.
Johansson, Å., Waight, T., Andersen, T., Simonsen, S.L., 2016. Geochemistry and petrogenesis of Mesoproterozoic A-type granitoids from the Danish island of Bornholm, southern Fennoscandia. Lithos 244, 94–108. https://doi.org/10.1016/j.lithos.2015.11.031.
Johnston, D.T., Poulton, S.W., Goldberg, T., Sergeev, V.N., Podkovyrov, V., Vorobieva, N.G., Bekker, A., Knoll, A.H., 2012. Late Ediacaran redox stability and metazoan evolution. Earth Planet. Sci. Lett. 335–336, 25–35. https://doi.org/10.1016/j.epsl.2012.05.010.
Kamber, B.S., Webb, G.E., 2001. The geochemistry of late Archaean microbial carbonate: implications for ocean chemistry and continental erosion history. Geochim. Cosmochim. Acta 65, 2509–2525. https://doi.org/10.1016/S0016-7037(01)00613-5.
Kechiched, R., Laouar, R., Bruguier, O., Laouar-Salmi, S., Ameur-Zaimeche, O., Foufou, A., 2016. Preliminary data of REE in Algerian phosphorites: a comparative study and paleo-redox insights. Procedia Eng. 138, 19–29. https://doi.org/10.1016/j.proeng.2016.02.048.
Khan, K.F., Dar, S.A., Khan, S.A., 2012. Rare earth element (REE) geochemistry of phosphorites of the Sonrai area of Paleoproterozoic Bijawar basin, Uttar Pradesh, India. J. Rare Earths 30, 507–514. https://doi.org/10.1016/S1002-0721(12)60081-7.
Khan, S.A., Khan, K.F., Dar, S.A., 2016. REE geochemistry of early Cambrian phosphorites of Masrana and Kimoi blocks, Uttarakhand, India. Arab. J. Geosci. 9, 456–465. https://doi.org/10.1007/s12517-016-2477-8.
Kidder, D.L., Eddy-Dillek, C.A., 1994. Rare-earth element variation in phosphate nodules from midcontinent Penssylvanian cyclothems. J. Sediment. Res. 64, 584–592. https://doi.org/10.1306/D4267E15-2B26-11D7-8648000102C1865D.
Kidder, D.L., Krishnaswamy, R., Mapes, R.H., 2003. Elemental mobility in phosphatic shales during concretion growth and implications for provenance analysis. Chem. Geol. 198, 335–353. https://doi.org/10.1016/S0009-2541(03)00036-6.
Kim, J., Torres, M.E., Haley, B.A., Kastner, M., Pohlman, J.W., Riedel, M., Lee, Y., 2012. The effect of diagenesis and fluid migration on rare earth element distribution in pore fluids of the northern Cascadia accretionary margin. Chem. Geol. 291, 152–165. https://doi.org/10.1016/j.chemgeo.2011.10.010.
Kopeliovich, A.V., 1965. Epigenesis of ancient sedimentary deposits from the southwestern part of the Russian Platform. Geol. J. RAS 121, 1–310 (in Russian).
Kostitsyn, Y.A., Volkov, V.N., Zhuravlev, D.Z., 2007. Trace elements and evolution of granite melt as exemplified by the Raumid Pluton, Southern Pamirs. Geochem. Int. 45, 1057–1069. https://doi.org/10.1134/S0016702907100023.
Lécuyer, C., Grandjean, P., Barrat, J.A., Nolvak, J., Emig, C., Paris, F., Robardet, M., 1998. δ18O and REE contents of phosphatic brachiopods: a comparison between modern and lower Paleozoic populations. Geochim. Cosmochim. Acta 62, 2429–2436. https://doi.org/10.1016/S0016-7037(98)00170-7.
Li, Z.-X., Evans, D.A.D., Halverson, G.P., 2013. Neoproterozoic glaciations in a revised global palaeogeography from the breakup of Rodinia to the assembly of Gondwanaland. Sediment. Geol. 294, 219–232. https://doi.org/10.1016/j.sedgeo.2013.05.016.
Mazumdara, A., Banerjee, D.M., Schidlowski, M., Balaram, V., 1999. Rare-earth elements and stable isotope geochemistry of early Cambrian chert-phosphorite assemblages from the Lower Tal Formation of the Krol Belt (Lesser Himalaya, India). Chem. Geol. 156, 275–297. https://doi.org/10.1016/S0009-2541(98)00187-9.
McArthur, J.M., 1985. Francolite geochemistry – compositional controls during formation, diagenesis, metamorphism and weathering. Geochim. Cosmochim. Acta 49, 23–35. https://doi.org/10.1016/0016-7037(85)90188-7.
McArthur, J.M., Walsh, J.N., 1984. Rare-earth geochemis try of phosphorites. Chem. Geol. 47, 191–220. https://doi.org/10.1016/0009-2541(84)90126-8.
McLennan, S.M., 2001. Relationships between the trace element composition of sedimentary rocks and upper continental crust. Geochem. Geophys. Geosystems 2, 1–24. https://doi.org/10.1029/2000GC000109.
McLennan, S.M., Nance, W.B., Taylor, S.R., 1980. Rare earth element–thorium correlation in sedimentary rocks, and the composition of the continental crust. Geochim. Cosmochim. Acta 44, 1833–1839. https://doi.org/10.1016/0016-7037(80)90232-X.
McLennan, S.M., Hemming, S., McDaniel, D.K., Hanson, G.N., 1993. Geochemical approaches to sedimentation, provenance and tectonics. Geol. Soc. Am. Special Paper 284, 21–40. https://doi.org/10.1130/SPE284-p21.
Meinhold, G., Jensen, S., Hoyberget, M., Arslan, A., Ebbestad, J.O., Hostrom, A.E.S., Palacios, T., Agic, H., Taylor, W.L., 2019. First record of carbonates with spherulites and cone-in-cone structures from the Precambrian of Arctic Norway, and their palaeoenvironmental significance. Precambrian Res. 328, 99–110. https://doi.org/10.1016/j.precamres.2019.04.014.
Mortelmans, G., 1957. Traces fossiles de vie dans les argilites lukuguiennes de Vuele Nyoka, de Luena-Kisulu et de la Lovoy (Katanga). Bulletin des Seances 3, 607–627.
Murthy, R., Kidder, D., Mapes, R., Hannigan, R., 2004. Rare-earth element chemistry of Mississippian–age phosphate nodules in the Fayetteville Shale of Oklahoma and Arkansas. Environ. Geosci. 11, 99–111. https://doi.org/10.1306/eg.01080403018.
Nosova, A.A., Kuzmenkova, O.F., Veretennikov, N.V., Petrova, L.G., Levsky, L.K., 2008. Neoproterozoic Volhynia–Brest magmatic province in the western East European craton: within-plate magmatism in an ancient suture zone. Petrology 16, 115–147. https://doi.org/10.1134/S086959110802001X.
Nozaki, Y., 2001. Rare earth element and their isotopes in the ocean. In: Steele, J.H., Thorpe, S.A., Turekian, K.K. (Eds.), Encyclopedia of Ocean Sciences. Academic Press, London, pp. 2354–2366.
Nozaki, Y., Zhang, J., Amakawa, H., 1997. The fractionation between Y and Ho in the marine environment. Earth Planet. Sci. Lett. 148, 329–340. https://doi.org/10.1016/S0012-821X(97)00034-4.
Öztürk, H., Hanilçi, N., Altuncu, S., Kasapçi, C., 2019. Rare earth element (REE) resources of Turkey: an overview of their characteristics and origin. Bull. Miner. Res. Explor. 159, 129–143. https://doi.org/10.19111/bulletinofmre.471205.
Palij, V.M., 1976. Remains of non-skeletal fauna and traces of life activity from upper Precambrian and lower Cambrian sediments of Podolia. In: Rjabenko, V.A., Velikanov, V.A., Aseeva, E.A., Palij, V.M., Tzegeliniuk, P.D., Zernetzkaja, N.V. (Eds.), Paleontology and Stratigraphy of the Upper Precambrian and Lower Paleozoic from the south-western part of the East-European Platform. Naukova Dumka, Kiev, pp. 63–77 (in Russian).

Palij, V.M., Posti, E., Fedonkin, M.A., 1979. Soft-bodied Metazoa and trace fossils of Vendian and lower Cambrian. In: Keller, B.M., Rozanov, A.Y. (Eds.), Upper Precambrian and Cambrian Paleontology of East-European Platform. Nauka, Moscow, pp. 49–82 (in Russian).

Patrulius, D., Iordan, M., 1974. On the occurrence of the pogonophore *Sabellidites cambriensis* Ian. and the sea-weed *Vendotaenia antiqua* Gnil. in the Pre-Silurian detrital rocks of the Moldavian Plateau. Institutul Geologic, Dări de seamă ale ședințelor 60/4, 1–18 (in Romanian).

Reynard, B., Lécuyer, C., Grandjean, P., 1999. Crystal-chemical controls on rare-earth element concentrations in fossil biogenic apatites and implications for paleoenvironmental reconstructions. Chem. Geol. 155, 233–241. https://doi.org/10.1016/S0009-2541(98)00169-7.

Rossel, P., Oliveros, V., Ducea, M.N., Charrier, R., Scaillet, S., Retamal, L., Figueroa, O., 2013. The Early Andean subduction system as an analog to island arcs: evidence from across-arc geochemical variations in northern Chile. Lithos 179, 211–230. https://doi.org/10.1016/j.lithos.2013.08.014.

Rudnick, R.L., Gao, S., 2003. Composition of the continental crust. Treatise Geochem. 3, 1–64. https://doi.org/10.1016/B0-08-043751-6/03016-4.

Shumlyanskyy, L.V., 2012. The evolution of the Vendian continental flood basalt magmatism in the Volyn region. Mineral. J. (Ukraine) 34, 50–68 (in Ukrainian).

Shumlyanskyy, L.V., Andréasson, P.G., Buchan, K.L., Ernst, R.E., 2007. The Volynian Flood Basalt Province and coeval (Ediacaran) magmatism in Baltoscandia and Laurentia. Mineral. J. (Ukraine) 29 (4), 47–55.

Shumlyanskyy, L., Nosova, A., Billström, K., Söderlund, U., Andréasson, P.-G., Kuzmenkova, O., 2016. The U-Pb zircon and baddeleyite ages of the Neoproterozoic Volyn Large Igneous Province: implication for the age of the magmatism and the nature of a crustal contaminant. GFF 138, 17–30. https://doi.org/10.1080/11035897.2015.1123289.

Shumlyanskyy, L.V., Stepanyuk, L.M., Claessen, S., Rudenko, K.V., Bekker, A.Y., 2018. U-Pb zircon and monazite geochronology of granitoids of the Zhytomyr and Sheremetiv complexes, Northwestern region of the Ukrainian Shield. Mineral. J. (Ukraine) 40, 63–85 (in Ukrainian).

Sokur, T.M., 2010. Diagenetic kaolinite and carbonate mineralization in the Vendian argillites on the southwestern slope of the East European Platform as indicator of petrogenesis. Litologija, Geologija morei i okeanov. Collection of Scientific Works of the Institute of Geological Sciences NAS of Ukraine 3, 138–142 (in Russian).

Sokur, T.M., 2011. Petrogenesis characteristics of argillites from the Vendian Kalyus Beds on the southwestern part of the East European Platform. Lett. Ukrainian Mineral. Soc. 8, 192–195 (in Russian).

Sokur, T.M., Figura, L.A., 2009. Diagenetic kaolinite mineralization in the Vendian argillites on the southwestern slope of the Ukrainian Shield. Litologija, Geologija morei i okeanov. Collection of Scientific Works of the Institute of Geological Sciences NAS of Ukraine 2, 147–151 (in Russian).

Soldatenko, Y., El Albani, A., Ruzina, M., Fontaine, C., Nesterovsky, V., Paquette, J.-L., Meunier, A., Ovtcharova, M., 2019. Precise U-Pb age constrains on the Ediacaran biota in Podolia, East European Platform, Ukraine. Nat. Sci. Rep. 9, 1–13. https://doi.org/10.1038/s41598-018-38448-9.

Srodon, J., Kuzmenkova, O., Stanek, J.J., Petit, S., Beaufort, D., Albert Gilg, H., Liivamagi, S., Goryl, M., Marynowski, L., Szczerba, M., 2019. Hydrothermal alteration of the Ediacaran Volyn-Brest volcanics on the western margin of the East European Craton. Precambrian Res. 217–235. https://doi.org/10.1016/j.precamres.2019.02.015.

Taylor, S.R., McLennan, S.M., 1985. The Continental Crust: Its Composition and Evolution. Blackwell, Oxford, pp. 1–312.

Tribovillard, N., Algeo, T.J., Lyons, T.W., Riboulleau, A., 2006. Application of trace metals as paleoredox and paleoproductivity proxies. Chem. Geol. 232, 12–32. https://doi.org/10.1016/j.chemgeo.2006.02.012.

Turekian, K.K., Wedepohl, K.H., 1961. Distribution of the elements in some major units of the earth's crust. GSA Bull. 72, 175–192. https://doi.org/10.1130/0016-7606(1961)72[175:DOTEIS]2.0.CO;2.

Văscăuțanu, T., 1931. Formațiunile siluriene din malul românesc al Nistrului – contribuțiuni la cunoașterea Paleozoicului din bazinul moldo-podolic. Les formations siluriennes de la rive roumaine du Dniester – contributions à la connaissance du Paléozoïque du basin moldo-podolique. Anuarul Institutului Geologic al României 15, 425–663 (in Romanian with French summary).

Văscăuțanu, T., Savul, M., 1927. Sur les phosphorites paléozoïque du Nord de la Bessarabie. Annales des Mines de Roumanie 10/1, 1–17.

Velikanov, V.A., 1979. Stratigraphic scheme of the southwestern part of the East European Platform in the Riphean and Vendian. Geol. J. 6, 54–66 (in Russian).

Velikanov, V.A., Aseeva, E.A., Fedonkin, M.A., 1983. Vendian of Ukraine. Naukova Dumka, Kiev, pp. 1–161 (in Russian).

Wang, W., Guan, C., Zhou, C., Peng, Y., Pratt, L.M., Chen, X., Chen, L., Chen, Z., Yuan, X., Xiao, S., 2016. Integrated carbon, sulfur, and nitrogen isotope chemostratigraphy of the Ediacaran Lantian Formation in South China: spatial gradient, ocean redox oscillation, and fossil distribution. Geobiology 15, 552–571. https://doi.org/10.1111/gbi.12226.

Whitney, D.L., Evans, B.W., 2010. Abbreviations for names of rock-forming minerals. Am. Mineral. 95, 185–187. https://doi.org/10.2138/am.2010.3371.

Wood, A., 1935. The origin of the structure known as *Guilielmites*. Geol. Mag. 72, 240–245.

Wood, R.A., Poulton, S.W., Prave, A.R., Hoffmann, K.H., Clarkson, M.O., Guilbaud, R., Lyne, J.W., Tostevin, R., Bowyer, F., Penny, A.M., Curtis, A., Kasemann, S.A., 2015. Dynamic redox conditions control late Ediacaran metazoan ecosystems in the Nama group, Namibia. Precambrian Res. 261, 252–271. https://doi.org/10.1016/j.precamres.2015.02.004.

Wright, J., Schrarder, H., Holser, W.T., 1987. Paleoredox variations in ancient oceans recorded by rare earth elements in fossil apatite. Geochim. Cosmochim. Acta 51, 631–644. https://doi.org/10.1016/0016-7037(87)90075-5.

Xin, H., Jiang, S., Yang, J., Wu, H., Pi, D.H., 2016. Rare earth element geochemistry of phosphatic rocks in Neoproterozoic Ediacaran Doushantuo Formation in Hushan section from the Yangtze Gorges area, South China. J. Earth Sci. 27, 204–210. https://doi.org/10.1007/s12583-015-0653-5.

Zaika-Novatsky, V.S., Palij, V.M., 1974. The oldest fossil fauna from the Vendian complex of Transnistria. Paleontol. J. RAS 11, 59–65 (in Russian).

Zhang, J., Amakawa, H., Nozaki, Y., 1994. The comparative behaviors of yttrium and lanthanides in the seawater of the North Pacific. Geophys. Res. Lett. 21, 2677–2680. https://doi.org/10.1029/94GL02404.

Zhang, L., Algeo, T.J., Cao, L., Zhao, L., Chen, Z.-Q., Li, Z., 2016. Diagenetic uptake of rare earth elements by conodont apatite. Palaeogeogr. Palaeoclimatol. Palaeoecol. 458, 176–197. https://doi.org/10.1016/j.palaeo.2015.10.049.

Zhang, F., Xiao, S., Kendall, B., Romaniello, S.J., Cui, H., Meyer, M., Gilleaudeau, G.J., Kaufman, A.J., Anbar, A.D., 2018. Extensive marine anoxia during the terminal Ediacaran Period. Sci. Adv. 6, 1–11. https://doi.org/10.1126/sciadv.aan8983.

Zhao, L., Chen, Z.-Q., Algeo, T.J., Chen, J., Chen, Y., Tong, J., Gao, S., Zhou, L., Hu, Z., Liu, Y., 2013. Rare-earth element patterns in conodont albid crowns: evidence for massive inputs of volcanic ash during the latest Permian biocrisis? Glob. Planet. Change 105, 135–151. https://doi.org/10.1016/j.gloplacha.2012.09.001.

Zhou, M.-F., Robinson, P.T., Lesher, C.M., Keays, R.R., Zhang, C.-J., Malpas, J., 2005. Geochemistry, petrogenesis and metallogenesis of the Panzhihua Gabbroic Layered Intrusion and associated Fe–Ti–V oxide deposits, Sichuan Province, SW China. J. Petrol. 46, 2253–2280. https://doi.org/10.1093/petrology/egi054.

Zhu, B., Jiang, S.-Y., Yang, J.-H., Pi, D., Ling, H.-F., Chen, Y.-Q., 2014. Rare earth element and Sr\Nd isotope geochemistry of phosphate nodules from the lower Cambrian Niutitang Formation, NW Hunan Province, South China. Palaeogeogr. Palaeoclimatol. Palaeoecol. 398, 132–143. https://doi.org/10.1016/j.palaeo.2013.10.002.